The dynamic stiffness matrix based on the extended separation-of-variables type solutions for the free vibration of orthotropic rectangular thin plates

Shiyi Mei[a], Colin Caprani[a,*], Daniel Cantero[b]

[a] *Department of Civil Engineering, Monash University, Melbourne, Victoria, Australia*
[b] *Department of Structural Engineering, Norwegian University of Science & Technology NTNU, Trondheim, Norway*

Abstract

The dynamic stiffness matrix based on the extended separation-of-variables mode functions is developed for the free vibration analysis of an orthotropic rectangular thin plate with general homogeneous boundary conditions. The governing differential equation and boundary conditions are derived from Rayleigh's principle. Based on the boundary conditions, the dynamic stiffness matrix is formulated and solved using an improved Wittrick-Williams algorithm. In this improved algorithm, simply supported frequencies are required instead of fully clamped frequencies, and the closed-form expression for the simply supported frequencies is provided, enhancing the efficiency and systematicity of solving the eigenvalue problem. The proposed method is validated by the numerical experiments.

1. Introduction

Rectangular plates play an important role in various engineering fields, including civil, mechanical, and aerospace engineering [3]. The free vibration of plates has been a fundamental research problem for over two centuries. The earliest exact solutions for this problem are the Navier [21] and Levy [14] solutions, which require at least one pair of opposite edges to be simply

*Corresponding author

Email addresses: `shiyi.mei1@monash.edu` (Shiyi Mei), `colin.caprani@monash.edu` (Colin Caprani), `daniel.cantero@ntnu.no` (Daniel Cantero)

supported or guided. To solve problems with other boundary conditions, approximate solutions such as the Rayleigh–Ritz method [13] and the Galerkin method [12] have been widely applied. For these approximation methods, beam functions, polynomials, trigonometric functions, and their combinations [16] are commonly used as the assumed approximate functions. The accuracy of these solutions depends on how well the assumed approximate functions represent the displacement of the plate.

Besides the approximation methods, several analytical methods have been developed over the past decades, including the Kantorovich-Krylov method [9, 10], the symplectic eigenfunction expansion method [32, 25], the separation-of-variable (SOV) method [29], the dynamic stiffness matrix (DSM) method [2], and series expansion-based methods [24]. The series expansion-based methods include the superposition method [22, 7], Fourier series method [11, 17], the finite integral transform method [15, 33], and other series methods. These methods represent the plate displacement in terms of an infinite series and mostly are capable of handling any general boundary conditions. However, sufficient truncation of the series is required to ensure the accuracy and convergence of the results, and the eigenvalue equation is generally difficult to express explicitly. Therefore, solving the corresponding eigenvalue problem can be computationally expensive.

Despite being a powerful method for the dynamic analysis of plate assemblies, the finite element method (FEM) requires a sufficient number of elements and is computationally expensive to accurately capture higher-order modes. Thus, the DSM method is developed as an accurate and efficient analytical approach to alternatively solve complex plate structures [4, 5]. The DSM can be considered as an analytical FEM since the mode functions of the plate are expressed by analytical solutions, where Levy-type solution [6] or components of infinite Fourier series [1, 19] are applied. To avoid solving the cumbersome transcendental frequency equation directly, the Wittrick-Williams (W-W) algorithm [23] is applied to the eigenvalue problem. The W-W algorithm determines the lower and upper bounds of natural frequencies rather than solving the frequency equation directly. Thus, the DSM has the potential to be effectively and systematically solved using the W-W algorithm. However, a critical part in applying the W-W algorithm is to priorly determine all natural frequencies of the fully clamped structure within the interested frequency range. Strategies such as using a sufficiently fine mesh or including a sufficient number of terms in series expansions [1] can ensure that all fully clamped frequencies are accounted for, thereby maintaining the accuracy of the algorithm. However, these approaches are computationally expensive and complex, posing a significant obstacle to the wider adoption and application of the DSM method based on the W-W algorithm [8]. To resolve the fully clamped plate problem, Liu and Banerjee [18] suggested that the fully clamped frequencies can be indirectly obtained from the simply supported plate problem, where the Navier solution serves as the analytical solution. This provides a significant enhancement to the W-W algorithm, increasing the efficiency of applying DSM methods. However, since infinite-term series expansion-based solutions are used for plate analysis instead of explicit and closed-form solutions, a sufficient number of truncation terms is required to ensure accuracy and capture the necessary modal degrees.

Inspired by the Navier and Levy solutions, Xing and Liu [29] proposed the separation-of-variables (SOV) method, which provides concise and explicit eigensolutions. The mode shape function has a separable form, $\phi(x)\psi(y)$, requiring only one $\phi(x)$ and one $\psi(y)$ for each mode order, allowing each eigenvalue equation to be explicitly expressed. However, this SOV method is not suitable to deal with plate with free boundary conditions. Therefore, an extended SOV method [26, 27] based on the Rayleigh quotient is proposed to accommodate plates with all classical boundary conditions, i.e., simply supported, clamped, guided, and free. Based on the Rayleigh quotient model, alternative iterative and improved SOV methods have been subsequently proposed [28]. Although SOV methods provide concise closed-form analytical solutions, solving the highly nonlinear eigenvalue equations is required.

In this study, the free vibration of orthotropic plates with general boundary conditions is analyzed by extending the SOV method based on the Rayleigh quotient to obtain the solution for elastically restrained plates. Subsequently, dynamic stiffness matrices in both the x and y directions, derived from the SOV-form solutions, are developed to solve the eigenvalue problem. By applying the 'hypothetical structure method', a modified W-W algorithm is developed, requiring only the natural frequencies of the simply supported structure instead of the necessity of fully clamped frequencies. The concise closed-form expression for the simply supported frequencies is directly obtained from the eigenvalue equation based on the SOV method, eliminating the extensive computational effort typically required in DSM methods to determine all fully clamped frequencies within the frequency range. Therefore, this approach can improve the systematic and effective application of the DSM method depending on the W-W algorithm. Alternatively, it can also be considered as an efficient technique for solving transcendental eigenvalue equations in the SOV method.

2. Mathematical model

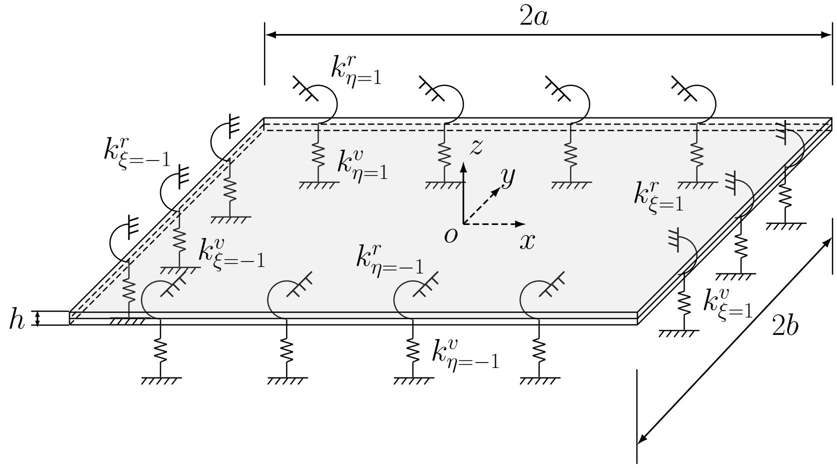

Figure 1: The orthotropic rectangular plate with all edges elastically restrained.

Consider a thin orthotropic rectangular plate of length $2a$ and width $2b$, with all four edges restrained by vertical translational springs k^v and rotational springs k^r, as shown in Figure 1. The coordinate origin is located at the center of the plate.

The governing differential equation for the free vibration of a thin orthotropic plate is given by [28]:

$$D_{11}\frac{\partial^4 w}{\partial \xi^4} + 2D_3\alpha^2\frac{\partial^4 w}{\partial \xi^2 \partial \eta^2} + D_{22}\alpha^4\frac{\partial^4 w}{\partial \eta^4} = \rho h \alpha^4 \omega^2 w, \tag{1}$$

where the bending stiffness parameters are defined as:

$$\begin{aligned} &D_{11} = \frac{E_1 h^3}{12(1 - v_{12}v_{21})}, \quad D_{22} = \frac{E_2 h^3}{12(1 - v_{12}v_{21})}, \\ &D_{66} = \frac{G_{12}h^3}{12}, \quad D_{12} = v_{12}D_{22} = v_{21}D_{11}, \quad D_3 = D_{12} + 2D_{66}, \end{aligned} \tag{2}$$

where ρ and h denote the mass density and thickness of the plate, respectively; E_1 and E_2 are the Young's moduli in the x- and y-directions, respectively; G_{12} is the shear modulus, and v_{12} and v_{21} are the Poisson's ratios.

Instead of solving the free vibration of the thin orthotropic plate using Equation (1), it is suggested that the vibration of the thin plate can also be solved using the Rayleigh quotient variational principle [26]:

$$\delta U_{mag} = \omega^2 \, \delta T_0, \tag{3}$$

where δ denotes variation, U_{mag} is the magnitude of the potential energy of the plate, and $\omega^2 T_0$ represents the magnitude of the kinetic energy of the plate. The potential energy of the plate can be expressed as [27]:

$$\begin{aligned} U^I = \frac{1}{2} \iint \Bigg[& D_{11} \left(\frac{\partial^2 W}{\partial x^2} \right)^2 + 2D_{12} \frac{\partial^2 W}{\partial x^2} \frac{\partial^2 W}{\partial y^2} + D_{22} \left(\frac{\partial^2 W}{\partial y^2} \right)^2 \\ & + 4D_{66} \left(\frac{\partial^2 W}{\partial x \partial y} \right)^2 \Bigg] \mathrm{d}x \, \mathrm{d}y. \end{aligned} \tag{4}$$

And the kinetic energy is:

$$T = \frac{1}{2} \iint \rho h \left(\frac{\partial W}{\partial t} \right)^2 \mathrm{d}x \, \mathrm{d}y. \tag{5}$$

Assuming the solution of the deflection $W(x, y; t) = w(x, y) e^{i\omega t}$ for harmonic plate motion, where $\mathrm{i} = \sqrt{-1}$, $w(x, y)$ is the mode shape, and ω is the radial frequency. By substituting $W(x, y; t) = w(x, y) e^{i\omega t}$ into Equations (4) and (5) and expressing the system in dimensionless coordinates, we have:

$$\begin{aligned} U^I_{\mathrm{mag}} = \frac{ab}{2} \iint \Bigg[& \frac{D_{11}}{a^4} \left(\frac{\partial^2 w}{\partial \xi^2} \right)^2 + \frac{2D_{12}}{a^2 b^2} \frac{\partial^2 w}{\partial \xi^2} \frac{\partial^2 w}{\partial \eta^2} + \frac{D_{22}}{b^4} \left(\frac{\partial^2 w}{\partial \eta^2} \right)^2 \\ & + \frac{4D_{66}}{a^2 b^2} \left(\frac{\partial^2 w}{\partial \xi \partial \eta} \right)^2 \Bigg] \mathrm{d}\xi \, \mathrm{d}\eta, \end{aligned} \tag{6}$$

and

$$T = \omega^2 \frac{ab}{2} \rho h \iint w^2 \, \mathrm{d}\xi \, \mathrm{d}\eta = \omega^2 T_0, \tag{7}$$

where $\alpha = a/b$ is the aspect ratio; $\xi = x/a$ and $\eta = y/b$ are the normalized coordinates. The separable form of the mode shape function $w(\xi, \eta)$ is given by:

$$w(\xi, \eta) = \phi(\xi) \psi(\eta), \tag{8}$$

where $\phi(\xi)$ and $\psi(\eta)$ can be expressed as:

$$\phi(\xi) = A_1 \sin(\alpha_1 \xi) + A_2 \cos(\alpha_1 \xi) + A_3 \sinh(\beta_1 \xi) + A_4 \cosh(\beta_1 \xi), \tag{9a}$$

$$\psi(\eta) = B_1 \sin(\alpha_2 \eta) + B_2 \cos(\alpha_2 \eta) + B_3 \sinh(\beta_2 \eta) + B_4 \cosh(\beta_2 \eta). \tag{9b}$$

It should be noted that Equation (1) represents the strong-form governing equation of the orthotropic plate, while Equation (3) is the weak-form governing equation, with the latter being equivalent to the former. Based on Equation (3), the frequencies ω_x and ω_y, corresponding to the mode shapes $\phi(\xi)$ and $\psi(\eta)$, respectively, are assumed to be independent of each other.

2.1. Dynamic stiffness matrix corresponding to ω_x

For given general homogeneous boundary conditions, we can first assume that the mode shape $\psi(\eta)$ corresponding to the y direction is known. Supposing the edges of the plate in both the x- and y-directions are elastically restrained by homogeneous vertical translational and rotational springs. The vertical translational and rotational springs at the $\xi = -1$ end are defined as $k^v_{\xi=-1}$ and $k^r_{\xi=-1}$, respectively, and at the $\xi = 1$ end as $k^v_{\xi=1}$ and $k^r_{\xi=1}$, respectively. Thus, the potential energy along the supported edge in the x-direction can be expressed by:

$$\begin{aligned} U^{II} = &\int \left[k^r_{\xi=-1} \left(\frac{\partial W}{\partial x} \right)^2 + k^v_{\xi=-1} (W)^2 \right]_{x=-a} \mathrm{d}y \\ &+ \int \left[k^r_{\xi=1} \left(\frac{\partial W}{\partial x} \right)^2 + k^v_{\xi=1} (W)^2 \right]_{x=a} \mathrm{d}y. \end{aligned} \tag{10}$$

From Equation (10), the magnitude of total potential energy along the edges in the x-direction is obtained as:

$$\begin{aligned} U^{II}_{mag} = ab &\int \left[\frac{k^r_{\xi=-1}}{a^3} \left(\frac{\partial w}{\partial \xi} \right)^2 + \frac{k^v_{\xi=-1}}{a} (w)^2 \right]_{\xi=-1} \mathrm{d}\eta \\ + ab &\int \left[\frac{k^r_{\xi=1}}{a^3} \left(\frac{\partial w}{\partial \xi} \right)^2 + \frac{k^v_{\xi=1}}{a} (w)^2 \right]_{\xi=1} \mathrm{d}\eta. \end{aligned} \tag{11}$$

The magnitude of potential energy of the plate in the x-direction can be obtained from Equations (6) and (11) as:

$$
\begin{aligned}
U_{mag} &= U_{mag}^{I} + U_{mag}^{II} \\
&= \frac{ab}{2} \iint \left[\frac{D_{11}}{a^4} \left(\frac{\partial^2 w}{\partial \xi^2} \right)^2 + \frac{2D_{12}}{a^2 b^2} \frac{\partial^2 w}{\partial \xi^2} \frac{\partial^2 w}{\partial \eta^2} + \frac{D_{22}}{b^4} \left(\frac{\partial^2 w}{\partial \eta^2} \right)^2 \right. \\
&\quad \left. + \frac{4D_{66}}{a^2 b^2} \left(\frac{\partial^2 w}{\partial \xi \partial \eta} \right)^2 \right] \mathrm{d}\xi \, \mathrm{d}\eta + ab \int \left[\frac{k^r_{\xi=1}}{a^3} \left(\frac{\partial w}{\partial \xi} \right)^2 + \frac{k^v_{\xi=1}}{a} (w)^2 \right]_{\xi=1} \mathrm{d}\eta \\
&\quad + ab \int \left[\frac{k^r_{\xi=-1}}{a^3} \left(\frac{\partial w}{\partial \xi} \right)^2 + \frac{k^v_{\xi=-1}}{a} (w)^2 \right]_{\xi=-1} \mathrm{d}\eta
\end{aligned}
\tag{12}
$$

By substituting Equation (8) into Equation (12), we have:

$$
\begin{aligned}
U_{mag} &= U_{mag}^{I} + U_{mag}^{II} \\
&= \frac{ab}{2} \int_{-1}^{1} \left[\frac{D_{11}}{a^4} S_1 \left(\frac{\mathrm{d}^2 \phi}{\mathrm{d}\xi^2} \right)^2 + \frac{2D_{12}}{a^2 b^2} S_2 \frac{\mathrm{d}^2 \phi}{\mathrm{d}\xi^2} \phi + \frac{D_{22}}{b^4} S_4 \phi^2 \right. \\
&\quad \left. + \frac{4D_{66}}{a^2 b^2} S_3 \left(\frac{\mathrm{d}\phi}{\mathrm{d}\xi} \right)^2 \right] \mathrm{d}\xi + abS_1 \left[\frac{k^r_{\xi=-1}}{a^3} \left(\frac{\mathrm{d}\phi}{\mathrm{d}\xi} \right)^2 + \frac{k^v_{\xi=-1}}{a} (\phi)^2 \right]_{\xi=-1} \\
&\quad + abS_1 \left[\frac{k^r_{\xi=1}}{a^3} \left(\frac{\mathrm{d}\phi}{\mathrm{d}\xi} \right)^2 + \frac{k^v_{\xi=1}}{a} (\phi)^2 \right]_{\xi=1},
\end{aligned}
\tag{13}
$$

where the integral parameters are defined as:

$$
\begin{aligned}
S_1 &= \int_{-1}^{1} \psi^2 \, \mathrm{d}\eta, \\
S_2 &= \int_{-1}^{1} \left(\frac{\mathrm{d}^2 \psi}{\mathrm{d}\eta^2} \psi \right) \mathrm{d}\eta, \\
S_3 &= \int_{-1}^{1} \left(\frac{\mathrm{d}\psi}{\mathrm{d}\eta} \right)^2 \mathrm{d}\eta, \\
S_4 &= \int_{-1}^{1} \left(\frac{\mathrm{d}^2 \psi}{\mathrm{d}\eta^2} \right)^2 \mathrm{d}\eta.
\end{aligned}
\tag{14}
$$

By taking Equation (8) into account, the coefficient T_0 of the kinetic energy in Equation (7) for the plate can be expressed as:

$$T_0 = \frac{ab}{2}\rho h \iint w^2 \, \mathrm{d}\xi \, \mathrm{d}\eta = \frac{ab}{2}\rho h S_1 \int_{-1}^{1} \phi^2 \, \mathrm{d}\xi. \tag{15}$$

Take the Rayleigh principle in the form:

$$\delta U_{mag} = \omega_x^2 \, \delta T_0. \tag{16}$$

By substituting Equations (13) and (15) into Equation (16), relieve $\delta\phi$ and $\delta\frac{\mathrm{d}\phi}{\mathrm{d}\xi}$ in Equation (16) by variation calculus, yielding:

$$\begin{aligned} 0 = &\int_{-1}^{1} \left[\frac{D_{11}}{a^4} S_1 \frac{\mathrm{d}^4\phi}{\mathrm{d}\xi^4} + \left(\frac{2D_{12}}{a^2b^2} S_2 - \frac{4D_{66}}{a^2b^2} S_3 \right) \frac{\mathrm{d}^2\phi}{\mathrm{d}\xi^2} \right. \\ &\left. + \left(\frac{D_{22}}{b^4} S_4 - \omega_x^2 \rho h S_1 \right) \phi \right] \delta\phi \, \mathrm{d}\xi \\ &+ \frac{2k^v_{\xi=-1}}{a} S_1 \Big(\phi\delta\phi\Big)_{\xi=-1} + \frac{2k^v_{\xi=1}}{a} S_1 \Big(\phi\delta\phi\Big)_{\xi=1} \\ &+ \left[\left(\frac{4D_{66}}{a^2b^2} S_3 - \frac{D_{12}}{a^2b^2} S_2 \right) \frac{\mathrm{d}\phi}{\mathrm{d}\xi} - \frac{D_{11}}{a^4} S_1 \frac{\mathrm{d}^3\phi}{\mathrm{d}\xi^3} \right] \delta\phi \Big|_{\xi=-1}^{\xi=1} \\ &+ \left(\frac{D_{12}}{a^2b^2} S_2 \phi + \frac{D_{11}}{a^4} S_1 \frac{\mathrm{d}^2\phi}{\mathrm{d}\xi^2} \right) \delta \frac{\mathrm{d}\phi}{\mathrm{d}\xi} \Big|_{\xi=-1}^{\xi=1} \\ &+ \frac{2k^r_{\xi=-1}}{a^3} S_1 \left(\frac{\mathrm{d}\phi}{\mathrm{d}\xi} \delta \frac{\mathrm{d}\phi}{\mathrm{d}\xi} \right)_{\xi=-1} + \frac{2k^r_{\xi=1}}{a^3} S_1 \left(\frac{\mathrm{d}\phi}{\mathrm{d}\xi} \delta \frac{\mathrm{d}\phi}{\mathrm{d}\xi} \right)_{\xi=1}. \end{aligned} \tag{17}$$

Thus, the governing differential equation in the x-direction can be obtained from the integration part in Equation (17):

$$\frac{\mathrm{d}^4\phi}{\mathrm{d}\xi^4} + 2\alpha^2 \left(\frac{D_{12}S_2}{D_{11}S_1} - 2\frac{D_{66}S_3}{D_{11}S_1} \right) \frac{\mathrm{d}^2\phi}{\mathrm{d}\xi^2} + \left(\alpha^4 \frac{D_{22}S_4}{D_{11}S_1} - a^4\Omega_x^4 \right) \phi = 0, \tag{18}$$

where $\Omega_x = \sqrt[4]{\omega_x^2 \rho h / D_{11}}$. By substituting $\phi(\xi) = Ae^{\mu\xi}$ into Equation (18), yields:

$$\mu^4 + 2\alpha^2 \left(\frac{D_{12}S_2}{D_{11}S_1} - 2\frac{D_{66}S_3}{D_{11}S_1} \right) \mu^2 + \left(\alpha^4 \frac{D_{22}S_4}{D_{11}S_1} - a^4\Omega_x^4 \right) = 0. \tag{19}$$

The solution for μ can be expressed as:

$$\mu_{1,2} = \pm i\alpha_1, \qquad \mu_{3,4} = \pm\beta_1, \tag{20}$$

where,

$$\alpha_1 = \alpha\sqrt{\sqrt{\left(\frac{D_{12}S_2}{D_{11}S_1} - 2\frac{D_{66}S_3}{D_{11}S_1}\right)^2 - \frac{D_{22}S_4}{D_{11}S_1} + b^4\Omega_x^4} + \frac{D_{12}S_2}{D_{11}S_1} - 2\frac{D_{66}S_3}{D_{11}S_1}}, \tag{21a}$$

$$\beta_1 = \alpha\sqrt{\sqrt{\left(\frac{D_{12}S_2}{D_{11}S_1} - 2\frac{D_{66}S_3}{D_{11}S_1}\right)^2 - \frac{D_{22}S_4}{D_{11}S_1} + b^4\Omega_x^4} - \frac{D_{12}S_2}{D_{11}S_1} + 2\frac{D_{66}S_3}{D_{11}S_1}}. \tag{21b}$$

The boundary conditions along the edges in the x-direction can be obtained from the remaining $\delta\phi$ and $\delta\frac{\mathrm{d}\phi}{\mathrm{d}\xi}$ parts in Equation (17). The shear force equilibrium can be obtained from the $\delta\phi$ part:

$$\begin{split}\left[\left(\frac{4D_{66}}{a^2b^2}S_3 - \frac{D_{12}}{a^2b^2}S_2\right)\frac{\mathrm{d}\phi}{\mathrm{d}\xi} - \frac{D_{11}}{a^4}S_1\frac{\mathrm{d}^3\phi}{\mathrm{d}\xi^3}\right]\Bigg|_{\xi=-1}^{\xi=1} \\ + \frac{2k^v_{\xi=-1}}{a}S_1\left(\phi\right)_{\xi=-1} + \frac{2k^v_{\xi=1}}{a}S_1\left(\phi\right)_{\xi=1} = 0,\end{split} \tag{22}$$

and from the $\delta\frac{\mathrm{d}\phi}{\mathrm{d}\xi}$ part, the bending moment equilibrium:

$$\begin{split}\left(\frac{D_{12}}{a^2b^2}S_2\phi + \frac{D_{11}}{a^4}S_1\frac{\partial^2\phi}{\partial\xi^2}\right)\Bigg|_{\xi=-1}^{\xi=1} + \frac{2k^r_{\xi=-1}}{a^3}S_1\left(\frac{\partial\phi}{\partial\xi}\right)_{\xi=-1} \\ + \frac{2k^r_{\xi=1}}{a^3}S_1\left(\frac{\partial\phi}{\partial\xi}\right)_{\xi=1} = 0.\end{split} \tag{23}$$

Thus, we can obtain the shear force and bending moment equilibrium along the edges $\xi = -1$ and $\xi = 1$ from Equations (22) and (23), respectively, as:

$$\frac{\mathrm{d}^3\phi}{\mathrm{d}\xi^3} - \alpha^2\left(\frac{4D_{66}S_3}{D_{11}S_1} - \frac{D_{12}S_2}{D_{11}S_1}\right)\frac{\mathrm{d}\phi}{\mathrm{d}\xi} + \frac{2a^3k^v_{\xi=-1}}{D_{11}}\phi = 0, \qquad \xi = -1, \tag{24a}$$

$$\frac{\mathrm{d}^2\phi}{\mathrm{d}\xi^2} + \frac{\alpha^2D_{12}S_2}{D_{11}S_1}\phi - \frac{2ak^r_{\xi=-1}}{D_{11}}\frac{\mathrm{d}\phi}{\mathrm{d}\xi} = 0, \qquad \xi = -1, \tag{24b}$$

$$\frac{\mathrm{d}^3\phi}{\mathrm{d}\xi^3} - \alpha^2\left(\frac{4D_{66}S_3}{D_{11}S_1} - \frac{D_{12}S_2}{D_{11}S_1}\right)\frac{\mathrm{d}\phi}{\mathrm{d}\xi} - \frac{2a^3k^v_{\xi=1}}{D_{11}}\phi = 0, \qquad \xi = 1, \tag{24c}$$

$$\frac{\mathrm{d}^2\phi}{\mathrm{d}\xi^2} + \frac{\alpha^2D_{12}S_2}{D_{11}S_1}\phi + \frac{2ak^r_{\xi=1}}{D_{11}}\frac{\mathrm{d}\phi}{\mathrm{d}\xi} = 0, \qquad \xi = 1. \tag{24d}$$

Substituting Equation (9a) into Equation (24), and denoting $k_{\xi}^{v*} = \frac{2a^3 k_{\xi}^{v}}{D_{11}}$, $k_{\xi}^{r*} = \frac{2ak_{\xi}^{r}}{D_{11}}$, $\sin\alpha_1 = S_{\alpha_1}$, $\cos\alpha_1 = C_{\alpha_1}$, $\sinh\alpha_1 = Sh_{\alpha_1}$, $\cosh\alpha_1 = Ch_{\alpha_1}$, $\sin\beta_1 = S_{\beta_1}$, $\cos\beta_1 = C_{\beta_1}$, $\sinh\beta_1 = Sh_{\beta_1}$, and $\cosh\beta_1 = Ch_{\beta_1}$, we have:

$$\begin{bmatrix} \gamma_1 C_{\alpha_1} - k_{\xi=-1}^{v*} S_{\alpha_1} & \gamma_1 S_{\alpha_1} + k_{\xi=-1}^{v*} C_{\alpha_1} & \gamma_2 Ch_{\beta_1} - k_{\xi=-1}^{v*} Sh_{\beta_1} & -\gamma_2 Sh_{\beta_1} + k_{\xi=-1}^{v*} Ch_{\beta_1} \\ \gamma_3 S_{\alpha_1} + k_{\xi=-1}^{r*} \alpha_1 C_{\alpha_1} & -\gamma_3 C_{\alpha_1} + k_{\xi=-1}^{r*} \alpha_1 S_{\alpha_1} & \gamma_4 Sh_{\beta_1} + k_{\xi=-1}^{r*} \beta_1 Ch_{\beta_1} & -\gamma_4 Ch_{\beta_1} - k_{\xi=-1}^{r*} \beta_1 Sh_{\beta_1} \\ -\gamma_1 C_{\alpha_1} + k_{\xi=1}^{v*} S_{\alpha_1} & \gamma_1 S_{\alpha_1} + k_{\xi=1}^{v*} C_{\alpha_1} & -\gamma_2 Ch_{\beta_1} + k_{\xi=1}^{v*} Sh_{\beta_1} & -\gamma_2 Sh_{\beta_1} + k_{\xi=1}^{v*} Ch_{\beta_1} \\ \gamma_3 S_{\alpha_1} + k_{\xi=1}^{r*} \alpha_1 C_{\alpha_1} & \gamma_3 C_{\alpha_1} - k_{\xi=1}^{r*} \alpha_1 S_{\alpha_1} & \gamma_4 Sh_{\beta_1} + k_{\xi=1}^{r*} \beta_1 Ch_{\beta_1} & \gamma_4 Ch_{\beta_1} + k_{\xi=1}^{r*} \beta_1 Sh_{\beta_1} \end{bmatrix} \begin{Bmatrix} A_1 \\ A_2 \\ A_3 \\ A_4 \end{Bmatrix} = \begin{Bmatrix} 0 \\ 0 \\ 0 \\ 0 \end{Bmatrix}, \tag{25}$$

or,

$$\mathbf{R}_x \mathbf{A} = \mathbf{0}, \tag{26}$$

where,

$$\begin{aligned} \gamma_1 &= -\alpha_1^3 - \alpha^2 \left(\frac{4D_{66}S_3}{D_{11}S_1} - \frac{D_{12}S_2}{D_{11}S_1} \right) \alpha_1, \\ \gamma_2 &= \beta_1^3 - \alpha^2 \left(\frac{4D_{66}S_3}{D_{11}S_1} - \frac{D_{12}S_2}{D_{11}S_1} \right) \beta_1, \\ \gamma_3 &= -\alpha_1^2 + \frac{\alpha^2 D_{12}S_2}{D_{11}S_1}, \\ \gamma_4 &= \beta_1^2 + \frac{\alpha^2 D_{12}S_2}{D_{11}S_1}. \end{aligned} \tag{27}$$

Note that the classic boundary conditions can be obtained by selecting extremely large or small srping stiffness constants. For non-trivial solutions, the characteristic equation or eigenvalue equation is obtained from the determinant of the matrix $\mathbf{R}_x$ in Equation (26), which must be zero. However, solving these trancedental equations are cunmbersome and tedious, thus the DSM is introducted to avoid the ineffective computation.

To develop its dynamic stiffness matrix, with the help of Equation (9a), the vertical displacement and rotation corresponding to the mode shape $\phi(\xi)$

along the x-direction at edges $\xi = -1$ and $\xi = 1$ can be expressed as:

$$\begin{Bmatrix} \phi(\xi=-1) \\ \frac{\mathrm{d}\phi(\xi=-1)}{\mathrm{d}\xi} \\ \phi(\xi=1) \\ \frac{\mathrm{d}\phi(\xi=1)}{\mathrm{d}\xi} \end{Bmatrix} = \begin{bmatrix} -S_{\alpha_1} & C_{\alpha_1} & -Sh_{\beta_1} & Ch_{\beta_1} \\ \alpha_1 C_{\alpha_1}/a & \alpha_1 S_{\alpha_1}/a & \beta_1 Ch_{\beta_1}/a & -\beta_1 Sh_{\beta_1}/a \\ S_{\alpha_1} & C_{\alpha_1} & Sh_{\beta_1} & Ch_{\beta_1} \\ \alpha_1 C_{\alpha_1}/a & -\alpha_1 S_{\alpha_1}/a & \beta_1 Ch_{\beta_1}/a & \beta_1 Sh_{\beta_1}/a \end{bmatrix} \begin{Bmatrix} A_1 \\ A_2 \\ A_3 \\ A_4 \end{Bmatrix}, \tag{28}$$

or,

$$\delta_x = \mathbf{Q}_x \mathbf{A}. \tag{29}$$

Note that the eigenvector $\mathbf{A}$ can be expressed by multiplying the inverse matrix $\mathbf{Q}_x^{-1}$ on the left side of Equation (29), and then substituting $\mathbf{A}$ into Equation (26), we obtain:

$$\mathbf{R}_x \mathbf{A} = \mathbf{R}_x \mathbf{Q}_x^{-1} \delta_x = \mathbf{0}. \tag{30}$$

where the dynamic stiffness matrix, denoted as $\mathbf{K}_x = \mathbf{R}_x \mathbf{Q}_x^{-1}$, can be obtained from Equation (30). This matrix can be used to compute the natural frequencies of the system instead of solving the eigenvalue equation, and the method for the computation will be given in Section 3.

2.2. Dynamic stiffness matrix corresponding to ω_y

In this section, the mode shape $\phi(\xi)$ derived in *Section* 2.1 is utilized to obtain the dynamic stiffness matrix in the y-direction. The vertical translational and rotational springs at $\eta = -1$ are denoted as $k^v_{\eta=-1}$ and $k^r_{\eta=-1}$, respectively, while those at $\eta = 1$ are represented by $k^v_{\eta=1}$ and $k^r_{\eta=1}$.

Similarly, the potential energy along the edges in the y-direction is given by:

$$\begin{aligned} U^{III}_{mag} = {} & ab \int \left[\frac{k^r_{\eta=-1}}{a^3} \left(\frac{\partial w}{\partial \eta} \right)^2 + \frac{k^v_{\eta=-1}}{a} w^2 \right]_{\eta=-1} \mathrm{d}\xi \\ & + ab \int \left[\frac{k^r_{\eta=1}}{a^3} \left(\frac{\partial w}{\partial \eta} \right)^2 + \frac{k^v_{\eta=1}}{a} w^2 \right]_{\eta=1} \mathrm{d}\xi. \end{aligned} \tag{31}$$

The total potential energy of the plate in the y-direction can be determined from Equations (6) and (31) as:

$$
\begin{aligned}
U_{mag} &= U_{mag}^{I} + U_{mag}^{III} \\
&= \frac{ab}{2} \iint \left[\frac{D_{11}}{a^4} \left(\frac{\partial^2 w}{\partial \xi^2} \right)^2 + \frac{2D_{12}}{a^2 b^2} \frac{\partial^2 w}{\partial \xi^2} \frac{\partial^2 w}{\partial \eta^2} + \frac{D_{22}}{b^4} \left(\frac{\partial^2 w}{\partial \eta^2} \right)^2 \right. \\
&\quad \left. + \frac{4D_{66}}{a^2 b^2} \left(\frac{\partial^2 w}{\partial \xi \partial \eta} \right)^2 \right] \mathrm{d}\xi \, \mathrm{d}\eta + ab \int \left[\frac{k_{\eta=1}^{r}}{b^3} \left(\frac{\partial w}{\partial \eta} \right)^2 + \frac{k_{\eta=1}^{v}}{b} (w)^2 \right]_{\eta=1} \mathrm{d}\xi \\
&\quad + ab \int \left[\frac{k_{\eta=-1}^{r}}{b^3} \left(\frac{\partial w}{\partial \eta} \right)^2 + \frac{k_{\eta=-1}^{v}}{b} (w)^2 \right]_{\eta=-1} \mathrm{d}\xi.
\end{aligned}
\tag{32}
$$

By substituting Equation (8) into Equation (32), we obtain:

$$
\begin{aligned}
U_{mag} &= U_{mag}^{I} + U_{mag}^{III} \\
&= \frac{ab}{2} \int_{-1}^{1} \left[\frac{D_{11}}{a^4} T_4 \psi^2 + \frac{2D_{12}}{a^2 b^2} T_2 \frac{\mathrm{d}^2 \psi}{\mathrm{d}\eta^2} \psi + \frac{D_{22}}{b^4} T_1 \left(\frac{\mathrm{d}^2 \psi}{\mathrm{d}\eta^2} \right)^2 \right. \\
&\quad \left. + \frac{4D_{66}}{a^2 b^2} T_3 \left(\frac{\mathrm{d}\psi}{\mathrm{d}\eta} \right)^2 \right] \mathrm{d}\eta + ab \left[\frac{k_{\eta=1}^{r}}{b^3} T \left(\frac{\mathrm{d}\psi}{\mathrm{d}\eta} \right)^2 + \frac{k_{\eta=1}^{v}}{b} T_1 (\psi)^2 \right]_{\eta=1} \\
&\quad + ab \left[\frac{k_{\eta=-1}^{r}}{b^3} T \left(\frac{\mathrm{d}\psi}{\mathrm{d}\eta} \right)^2 + \frac{k_{\eta=-1}^{v}}{b} T_1 (\psi)^2 \right]_{\eta=-1},
\end{aligned}
\tag{33}
$$

where the integral parameters are defined as:

$$
\begin{aligned}
T_1 &= \int_{-1}^{1} \phi^2 \, \mathrm{d}\xi, \\
T_2 &= \int_{-1}^{1} \left(\frac{\mathrm{d}^2 \phi}{\mathrm{d}\xi^2} \phi \right) \mathrm{d}\xi, \\
T_3 &= \int_{-1}^{1} \left(\frac{\mathrm{d}\phi}{\mathrm{d}\xi} \right)^2 \mathrm{d}\xi, \\
T_4 &= \int_{-1}^{1} \left(\frac{\mathrm{d}^2 \phi}{\mathrm{d}\xi^2} \right)^2 \mathrm{d}\xi.
\end{aligned}
\tag{34}
$$

The coefficient T_0 of the kinetic energy in Equation (7) for the plate can be expressed as:

$$T_0 = \frac{ab}{2}\rho h T_1 \int_{-1}^{1} \psi^2 \,\mathrm{d}\eta. \tag{35}$$

Taking the Rayleigh principle in the form:

$$\delta U_{mag} = \omega_y^2 \,\delta T_0. \tag{36}$$

By substituting Equations (33) and (35) into Equation (36), and applying the variational calculus to eliminate $\delta\psi$ and $\delta\frac{\mathrm{d}\psi}{\mathrm{d}\eta}$ in Equation (36), we obtain:

$$\begin{aligned}
0 = &\int_{-1}^{1} \left[\frac{D_{22}}{b^4} T_1 \frac{d^4\psi}{\mathrm{d}\eta^4} + \left(\frac{2D_{12}}{a^2b^2} T_2 - \frac{4D_{66}}{a^2b^2} T_3 \right) \frac{\mathrm{d}^2\psi}{\mathrm{d}\eta^2} \right. \\
&\left. + \left(\frac{D_{11}}{a^4} T_4 - \omega_y^2 \rho h T_1 \right) \psi \right] \delta\psi \,\mathrm{d}\eta \\
&+ \frac{2k^v_{\eta=-1}}{b} T_1 (\psi\delta\psi)_{\eta=-1} + \frac{2k^v_{\eta=1}}{b} T_1 (\psi\delta\psi)_{\eta=1} \\
&+ \left[\left(\frac{4D_{66}}{a^2b^2} T_3 - \frac{D_{12}}{a^2b^2} T_2 \right) \frac{\mathrm{d}\psi}{\mathrm{d}\eta} - \frac{D_{22}}{b^4} T_1 \frac{\mathrm{d}^3\psi}{\mathrm{d}\eta^3} \right] \delta\psi \Big|_{\eta=-1}^{\eta=1} \\
&+ \left(\frac{D_{12}}{a^2b^2} T_2 \psi + \frac{D_{22}}{b^4} T_1 \frac{\mathrm{d}^2\psi}{\mathrm{d}\eta^2} \right) \delta \frac{\mathrm{d}\psi}{\mathrm{d}\eta} \Big|_{\eta=-1}^{\eta=1} \\
&+ \frac{2k^r_{\eta=-1}}{b^3} T_1 \left(\frac{\mathrm{d}\psi}{\mathrm{d}\eta} \delta \frac{\mathrm{d}\psi}{\mathrm{d}\eta} \right)_{\eta=-1} + \frac{2k^r_{\eta=1}}{b^3} T_1 \left(\frac{\mathrm{d}\psi}{\mathrm{d}\eta} \delta \frac{\mathrm{d}\psi}{\mathrm{d}\eta} \right)_{\eta=1}.
\end{aligned} \tag{37}$$

Thus, the governing differential equation in the y-direction can be obtained from the integration part in Equation (37):

$$\frac{\mathrm{d}^4\psi}{\mathrm{d}\eta^4} + \frac{2}{\alpha^2} \left(\frac{D_{12}T_2}{D_{22}T_1} - 2\frac{D_{66}T_3}{D_{22}T_1} \right) \frac{\mathrm{d}^2\psi}{\mathrm{d}\eta^2} + \left(\frac{D_{11}T_4}{\alpha^4 D_{22}T_1} - \frac{b^4 D_{11}}{D_{22}} \Omega_y^4 \right) \psi = 0, \tag{38}$$

where $\Omega_y = \sqrt[4]{\frac{\omega_y^2 \rho h}{D_{11}}}$. Substituting $\psi(\eta) = Be^{\lambda\eta}$ into Equation (38), yields:

$$\lambda^4 + \frac{2}{\alpha^2} \left(\frac{D_{12}T_2}{D_{22}T_1} - 2\frac{D_{66}T_3}{D_{22}T_1} \right) \lambda^2 + \left(\frac{D_{11}T_4}{\alpha^4 D_{22}T_1} - \frac{b^4 D_{11}}{D_{22}} \Omega_y^4 \right) = 0. \tag{39}$$

The solution for λ can be expressed as:

$$\lambda_{1,2} = \pm i\alpha_2, \qquad \lambda_{3,4} = \pm\beta_2, \tag{40}$$

where,

$$\alpha_2 = \frac{1}{\alpha}\sqrt{\sqrt{\left(\frac{D_{12}T_2}{D_{22}T_1} - 2\frac{D_{66}T_3}{D_{22}T_1}\right)^2 - \frac{D_{11}T_4}{D_{22}T_1} + \frac{a^4 D_{11}}{D_{22}}\Omega_y^4} + \frac{D_{12}T_2}{D_{22}T_1} - 2\frac{D_{66}T_3}{D_{22}T_1}}, \tag{41a}$$

$$\beta_2 = \frac{1}{\alpha}\sqrt{\sqrt{\left(\frac{D_{12}T_2}{D_{22}T_1} - 2\frac{D_{66}T_3}{D_{22}T_1}\right)^2 - \frac{D_{11}T_4}{D_{22}T_1} + \frac{a^4 D_{11}}{D_{22}}\Omega_y^4} - \frac{D_{12}T_2}{D_{22}T_1} + 2\frac{D_{66}T_3}{D_{22}T_1}}. \tag{41b}$$

The boundary conditions along the edges in the y-direction can be obtained from the remaining $\delta\psi$ and $\delta\frac{\mathrm{d}\psi}{\mathrm{d}\eta}$ parts in Equation (37). The shear force equilibrium can be obtained from the $\delta\psi$ part:

$$\begin{aligned}&\left[\left(\frac{4D_{66}}{a^2b^2}T_3 - \frac{D_{12}}{a^2b^2}T_2\right)\frac{\mathrm{d}\psi}{\mathrm{d}\eta} - \frac{D_{22}}{b^4}T_1\frac{\mathrm{d}^3\psi}{\mathrm{d}\eta^3}\right]\Bigg|_{\eta=-1}^{\eta=1} \\ &\quad + \frac{2k^v_{\eta=-1}}{b}T_1(\psi)_{\eta=-1} + \frac{2k^v_{\eta=1}}{b}T_1(\psi)_{\eta=1} = 0,\end{aligned} \tag{42}$$

and from the $\delta\frac{\mathrm{d}\psi}{\mathrm{d}\eta}$ part, the bending moment equilibrium:

$$\begin{aligned}&\left(\frac{D_{12}}{a^2b^2}T_2\psi + \frac{D_{22}}{b^4}T_1\frac{\mathrm{d}^2\psi}{\mathrm{d}\eta^2}\right)\Bigg|_{\eta=-1}^{\eta=1} + \frac{2k^r_{\eta=-1}}{b^3}T_1\left(\frac{\mathrm{d}\psi}{\mathrm{d}\eta}\right)_{\eta=-1} \\ &\qquad + \frac{2k^r_{\eta=1}}{b^3}T_1\left(\frac{\mathrm{d}\psi}{\mathrm{d}\eta}\right)_{\eta=1} = 0.\end{aligned} \tag{43}$$

Thus, we can obtain the shear force and bending moment equilibrium along the edges $\eta = -1$ and $\eta = 1$ from Equations (42) and (43), respectively, as:

$$\frac{\mathrm{d}^3\psi}{\mathrm{d}\eta^3} - \left(\frac{4D_{66}T_3}{\alpha^2 D_{22}T_1} - \frac{D_{12}T_2}{\alpha^2 D_{22}T_1}\right)\frac{\mathrm{d}\psi}{\mathrm{d}\eta} + \frac{2b^3k^v_{\eta=-1}}{D_{22}}\psi = 0, \qquad \eta = -1, \tag{44a}$$

$$\frac{\mathrm{d}^2\psi}{\mathrm{d}\eta^2} + \frac{D_{12}T_2}{\alpha^2 D_{22}T_1}\psi - \frac{2bk^r_{\eta=-1}}{D_{22}}\frac{\mathrm{d}\psi}{\mathrm{d}\eta} = 0, \qquad \eta = -1, \tag{44b}$$

$$\frac{\mathrm{d}^3\psi}{\mathrm{d}\eta^3} - \left(\frac{4D_{66}T_3}{\alpha^2 D_{22}T_1} - \frac{D_{12}T_2}{\alpha^2 D_{22}T_1}\right)\frac{\mathrm{d}\psi}{\mathrm{d}\eta} - \frac{2b^3k^v_{\eta=1}}{D_{22}}\psi = 0, \qquad \eta = 1, \tag{44c}$$

$$\frac{\mathrm{d}^2\psi}{\mathrm{d}\eta^2} + \frac{D_{12}T_2}{\alpha^2 D_{22}T_1}\psi + \frac{2bk^r_{\eta=1}}{D_{22}}\frac{\mathrm{d}\psi}{\mathrm{d}\eta} = 0, \qquad \eta = 1. \tag{44d}$$

Substituting Equation (9b) into Equation (44) and introducing the notations $k_{\eta}^{v*} = \frac{2b^3 k_{\eta}^{v}}{D_{22}}$, $k_{\eta}^{r*} = \frac{2bk_{\eta}^{r}}{D_{22}}$, $\sin\alpha_2 = S_{\alpha_2}$, $\cos\alpha_2 = C_{\alpha_2}$, $\sinh\alpha_2 = Sh_{\alpha_2}$, $\cosh\alpha_2 = Ch_{\alpha_2}$, $\sin\beta_2 = S_{\beta_2}$, $\cos\beta_2 = C_{\beta_2}$, $\sinh\beta_2 = Sh_{\beta_2}$, and $\cosh\beta_2 = Ch_{\beta_2}$, We obtain:

$$\begin{bmatrix} \hat{\gamma}_1 C_{\alpha_2} - k_{\eta=-1}^{v*} S_{\alpha_2} & \hat{\gamma}_1 S_{\alpha_2} + k_{\eta=-1}^{v*} C_{\alpha_2} & \hat{\gamma}_2 Ch_{\beta_2} - k_{\eta=-1}^{v*} Sh_{\beta_2} & -\hat{\gamma}_2 Sh_{\beta_2} + k_{\eta=-1}^{v*} Ch_{\beta_2} \\ \hat{\gamma}_3 S_{\alpha_2} + k_{\eta=-1}^{r*} \alpha_2 C_{\alpha_2} & -\hat{\gamma}_3 C_{\alpha_2} + k_{\eta=-1}^{r*} \alpha_2 S_{\alpha_2} & \hat{\gamma}_4 Sh_{\beta_2} + k_{\eta=-1}^{r*} \beta_2 Ch_{\beta_2} & -\hat{\gamma}_4 Ch_{\beta_2} - k_{\eta=-1}^{r*} \beta_2 Sh_{\beta_2} \\ -\hat{\gamma}_1 C_{\alpha_2} + k_{\eta=1}^{v*} S_{\alpha_2} & \hat{\gamma}_1 S_{\alpha_2} + k_{\eta=1}^{v*} C_{\alpha_2} & -\hat{\gamma}_2 Ch_{\beta_2} + k_{\eta=1}^{v*} Sh_{\beta_2} & -\hat{\gamma}_2 Sh_{\beta_2} + k_{\eta=1}^{v*} Ch_{\beta_2} \\ \hat{\gamma}_3 S_{\alpha_2} + k_{\eta=1}^{r*} \alpha_2 C_{\alpha_2} & \hat{\gamma}_3 C_{\alpha_2} - k_{\eta=1}^{r*} \alpha_2 S_{\alpha_2} & \hat{\gamma}_4 Sh_{\beta_2} + k_{\eta=1}^{r*} \beta_2 Ch_{\beta_2} & \hat{\gamma}_4 Ch_{\beta_2} + k_{\eta=1}^{r*} \beta_2 Sh_{\beta_2} \end{bmatrix} \begin{Bmatrix} B_1 \\ B_2 \\ B_3 \\ B_4 \end{Bmatrix} = \begin{Bmatrix} 0 \\ 0 \\ 0 \\ 0 \end{Bmatrix}, \tag{45}$$

or,

$$\mathbf{R}_y \mathbf{B} = \mathbf{0}, \tag{46}$$

where,

$$\begin{aligned} \hat{\gamma}_1 &= -\alpha_2^3 - \left(\frac{4D_{66}T_3}{\alpha^2 D_{22} T_1} - \frac{D_{12}T_2}{\alpha^2 D_{22} T_1} \right) \alpha_2, \\ \hat{\gamma}_2 &= \beta_2^3 - \left(\frac{4D_{66}T_3}{\alpha^2 D_{22} T_1} - \frac{D_{12}T_2}{\alpha^2 D_{22} T_1} \right) \beta_2, \\ \hat{\gamma}_3 &= -\alpha_2^2 + \frac{D_{12}T_2}{\alpha^2 D_{22} T_1}, \\ \hat{\gamma}_4 &= \beta_2^2 + \frac{D_{12}T_2}{\alpha^2 D_{22} T_1}. \end{aligned} \tag{47}$$

With the help of Equation (9b), the vertical displacement and rotation corresponding to the mode shape ψ along the y-direction at the edges $\eta = -1$ and $\eta = 1$ can be expressed as:

$$\begin{Bmatrix} \psi_{\eta=-1} \\ \frac{\mathrm{d}\psi}{\mathrm{d}\eta}_{\eta=-1} \\ \psi_{\eta=1} \\ \frac{\mathrm{d}\psi}{\mathrm{d}\eta}_{\eta=1} \end{Bmatrix} = \begin{bmatrix} -S_{\alpha_2} & C_{\alpha_2} & -Sh_{\beta_2} & Ch_{\beta_2} \\ \frac{\alpha_2 C_{\alpha_2}}{b} & \frac{\alpha_2 S_{\alpha_2}}{b} & \frac{\beta_2 Ch_{\beta_2}}{b} & -\frac{\beta_2 Sh_{\beta_2}}{b} \\ S_{\alpha_2} & C_{\alpha_2} & Sh_{\beta_2} & Ch_{\beta_2} \\ \frac{\alpha_2 C_{\alpha_2}}{b} & -\frac{\alpha_2 S_{\alpha_2}}{b} & \frac{\beta_2 Ch_{\beta_2}}{b} & \frac{\beta_2 Sh_{\beta_2}}{b} \end{bmatrix} \begin{Bmatrix} B_1 \\ B_2 \\ B_3 \\ B_4 \end{Bmatrix}, \tag{48}$$

or,

$$\delta_y = \mathbf{Q}_y \mathbf{B}. \tag{49}$$

Note that the eigenvector $\mathbf{B}$ can be expressed by multiplying the inverse matrix $\mathbf{Q}_y^{-1}$ on the left-hand side of Equation (49), and then substituting $\mathbf{B}$ into Equation (46), we obtain:

$$\mathbf{R}_y\mathbf{B} = \mathbf{R}_y\mathbf{Q}_x^{-1}\delta_y = \mathbf{0}, \tag{50}$$

where the dynamic stiffness matrix, denoted as $\mathbf{K}_y = \mathbf{R}_y\mathbf{Q}_y^{-1}$, can be obtained from Equation (50).

3. Frequency and mode shape computation

3.1. Wittrick–Williams algorithm

The Wittrick–Williams (W-W) algorithm [23] is an effective method for determining the natural frequencies from the dynamic stiffness matrix with high reliability. Instead of directly solving the equations, the algorithm computes the total number J of natural frequencies below a given frequency ω^*, which is represented as:

$$J(\omega^*) = J_0(\omega^*) + s\{\mathbf{K}^\Delta(\omega^*)\} = J_0(\omega^*) + J_k(\omega^*), \tag{51}$$

where J_0 represents the number of natural frequencies for the system with both ends fully clamped, $\mathbf{K}^\Delta$ is the upper triangular matrix obtained from the dynamic stiffness matrix $\mathbf{K}$ after applying Gaussian elimination, and $J_k(\omega^*)$ denotes the number of negative elements in the leading diagonal of $\mathbf{K}^\Delta$.

It should be noted that the J_0 count is a crucial aspect when applying the W-W algorithm. Many previous studies use a sufficiently fine mesh or enough terms in series expansions to capture all fully clamped natural frequencies, ensuring computational accuracy [1]. However, this approach can make the application process cumbersome. To address this issue, the fully clamped problem can be replaced with a simply supported problem, where the Navier solution for the simply supported plate is used to count J_0 [18]. Nevertheless, since analytical solutions in DSM methods involve an infinite series of Fourier terms, a sufficient number of truncation terms is required to ensure accuracy and convergence.

However, the idea of solving the simply supported problem proposes an effective and systematic approach to indirectly determine the J_0 count for a fully clamped structure using the 'hypothetical structure method', where the boundary conditions are modeled as pinned supports rather than clamped ones [8]:

$$J_0(p_1, \omega^*) = J(\bar{p}_1, \omega^*) - J_k(\bar{p}_1, \omega^*), \tag{52}$$

where p_1 and $\bar{p}_1$ represent clamped and pinned supports, respectively. By substituting Equation (52) into Equation (51) we get the algorithm as:

$$J(p, \omega^*) = J(\bar{p}_1, \omega^*) - J_k(\bar{p}_1, \omega^*) + J_k(p, \omega^*) \tag{53}$$

where p represents the original boundary conditions of the structure. Therefore, the challenge of determining $J_0(p_1, \omega^*)$ can be transformed into the problem of solving $J(\bar{p}_1, \omega^*)$ instead. The eigenvalue equation corresponding to the natural frequency parameter Ω_x can be obtained from the determinant of the coefficient matrix $\mathbf{R}_x$ in Equation (25), which is given by:

$$\sin 2\alpha_1 = 0. \tag{54}$$

With the help of Equations (21a) and (54), the closed-form solution of the n_xth simply supported frequency Ω_{x,n_x} for the given n_y-order $\psi_{n_y}(\eta)$ can be expressed as:

$$\Omega_{x,n_x} = \frac{1}{b}\sqrt[4]{\begin{aligned}&\left[\left(\frac{n_x\pi}{2\alpha}\right)^2 - \frac{D_{12}S_2}{D_{11}S_1} + 2\frac{D_{66}S_3}{D_{11}S_1}\right]^2 - \left(\frac{D_{12}S_2}{D_{11}S_1} - 2\frac{D_{66}S_3}{D_{11}S_1}\right)^2\\ &+ \frac{D_{22}S_4}{D_{11}S_1}.\end{aligned}} \tag{55}$$

For $\Omega_{x,n_x} \leq \Omega_x^* < \Omega_{x,n_{x+1}}$, $J(\bar{p}_1, \Omega_x^*) = n_x$. Similarly, the closed-form solution of the n_yth simply supported frequency Ω_{y,n_y} for the given n_x-order $\phi_{n_x}(\xi)$ can be expressed as:

$$\Omega_{y,n_y} = \frac{1}{a}\sqrt[4]{\begin{aligned}&\frac{D_{22}}{D_{11}}\left\{\left[\left(\frac{n_y\pi\alpha}{2}\right)^2 - \frac{D_{12}T_2}{D_{22}T_1} + 2\frac{D_{66}T_3}{D_{22}T_1}\right]^2 - \left(\frac{D_{12}T_2}{D_{22}T_1} - 2\frac{D_{66}T_3}{D_{22}T_1}\right)^2\right.\\ &\left.+\frac{D_{11}T_4}{D_{22}T_1}\right\}.\end{aligned}} \tag{56}$$

For $\Omega_{y,n_y} \leq \Omega_y^* < \Omega_{y,n_{y+1}}$, $J(\bar{p}_1, \Omega_y^*) = n_y$. According to the relationships $\Omega_x = \sqrt[4]{\frac{\omega_x^2\rho h}{D_{11}}}$ and $\Omega_y = \sqrt[4]{\frac{\omega_y^2\rho h}{D_{11}}}$, the values of $J(\bar{p}_1, \omega_x^*)$ and $J(\bar{p}_1, \omega_y^*)$ can be derived from $J(\bar{p}_1, \Omega_x^*)$ and $J(\bar{p}_1, \Omega_y^*)$, respectively. Therefore, this refined

W-W algorithm can be applied to estimate the lower and upper bounds of the frequency range, denoted as ω_l and ω_u, yielding an approximation for the frequency $\omega_a \in (\omega_l, \omega_u)$.

The mode shape coefficients A_1 to A_4 and B_1 to B_4 in the eigenvectors $\mathbf{A}$ and $\mathbf{B}$ for all classic boundary conditions are provided in [27]. Alternatively, these coefficients can also be obtained through a simple numerical method, which this work presents as an approach. Here, we illustrate solving the eigenvector $\mathbf{A}$ as an example. By assuming the exact natural frequency as ω_k, we can expand the coefficient matrix $\mathbf{R}_x$ in Equation (25) using a first-order Taylor series about ω_a:

$$\mathbf{R}_{x,k}(\omega_k)\mathbf{A}_k = \mathbf{R}_{x,a}\mathbf{A}_k + (\omega_k - \omega_a)\mathbf{R}'_{x,a}\mathbf{A}_k + O\left((\omega_k - \omega_a)^2\right) = 0. \tag{57}$$

Ignoring higher-order terms, an eigenvalue problem can be derived from Equation (57):

$$(\mathbf{R}'_{x,a})^{-1}\mathbf{R}_{x,a}\mathbf{A} = (\omega_a - \omega_k)\mathbf{A} = \tau\mathbf{A}. \tag{58}$$

This eigenvalue problem can be solved using the inverse iteration procedure [30]:

$$\bar{\mathbf{A}}^{(i+1)} = \mathbf{R}_{x,a}^{-1}\mathbf{R}'_{x,a}\mathbf{A}^{(i)}, \tag{59}$$

where the initial guess for $\mathbf{A}^{(0)}$ is a column vector consisting of four randomly generated elements, each of which falls within the range (0,1). The updated eigenvalue for the next step can be obtained as:

$$\tau^{(i+1)} = \frac{1}{\bar{A}_j^{(i+1)}}, \tag{60}$$

where,

$$\mid \bar{A}_j^{(i+1)} \mid = \max(\mid \bar{A}_1^{(i+1)} \mid, \mid \bar{A}_2^{(i+1)} \mid, \mid \bar{A}_3^{(i+1)} \mid, \mid \bar{A}_4^{(i+1)} \mid). \tag{61}$$

The updated eigenvector can be obtained as:

$$\mathbf{A}^{(i+1)} = \tau^{(i+1)}\bar{\mathbf{A}}^{(i+1)}. \tag{62}$$

The procedure can be controlled by the error tolerance ϵ or maximum allowed steps $i_{\max}$:

$$\max \mid A_n^{(i+1)} - A_n^{(i)} \mid < \epsilon, \tag{63a}$$

$$i = i_{\max}. \tag{63b}$$

Note that the mode shape coefficients A_1 to A_4 obtained from $\mathbf{A}^{(i+1)}$ are applied for the elastically restrained boundary conditions.

3.2. Application procedure

The procedure of the proposed method is as follows:

3.2.1. Iterative procedure

- **Step 1** Assume initial integral parameters $S_1^{(0)}, S_2^{(0)}, S_3^{(0)}$, and $S_4^{(0)}$ in the y-direction. Using the given boundary conditions (BCs) at $\xi = -1$ and $\xi = 1$, determine $\mathbf{K}_x^{(0)}$ from Equation (30). Then, apply the computational algorithms in Section 3.1 to compute the n_x-th frequency $\omega_{x,n_x}^{(0)}$ and its corresponding mode shape $\phi_{n_x}^{(0)}$, where $n_x = 1, 2, 3, \ldots$.

- **Step 2** Use $\phi_{n_x}^{(0)}$ as the prescribed mode to determine $\mathbf{K}_y^{(1)}$ in Equation (50), considering the BCs at $\eta = -1$ and $\eta = 1$. Apply the computational algorithms to obtain the n_y-th frequency $\omega_{y,n_y}^{(1)}$ and its corresponding mode shape $\psi_{n_y}^{(1)}$, where $n_y = 1, 2, 3, \ldots$. This completes the first iteration cycle.

- **Step 3** Use $\psi_{n_y}^{(1)}$ as the prescribed n_y-th mode shape in the y-direction to compute $\mathbf{K}_x^{(1)}$ from Equation (30), then determine the n_x-th frequency $\omega_{x,n_x}^{(1)}$ and its corresponding mode shape $\phi_{n_x}^{(1)}$.

- **Step 4** Use $\phi_{n_x}^{(1)}$ as the prescribed mode in the x-direction to compute the n_y-th frequency $\omega_{y,n_y}^{(2)}$ and its corresponding mode shape $\psi_{n_y}^{(2)}$, completing the second iteration cycle.

- **Step 5** Stop the iteration if $\mid \omega_{x,n_x}^{(i)} - \omega_{x,n_x}^{(i+1)} \mid \leq \Delta\omega$ or $\mid \omega_{y,n_y}^{(i)} - \omega_{y,n_y}^{(i+1)} \mid \leq \Delta\omega$, where $\Delta\omega$ is the frequency interval defined in Section 3, where, $\Delta\omega = \omega_u - \omega_l$.

- **Step 6** Finally, construct the (n_x, n_y)-th mode shape as $w(\xi, \eta) = \phi_{n_x}(\xi)\psi_{n_y}(\eta)$ using Equation (8).

3.2.2. Non-iterative Procedure

Although the iterative procedure in Section 3.2.1 can be used to obtain any desired mode, a non-iterative approach can enhance the efficiency of numerical calculations when an exact mode is known.

Once a nonzero mode shape $\phi_{n_x}(\xi)\psi_{n_y}(\eta)$ is determined by following the iterative procedure in Section 3.2.1, $\psi_{n_y}(\eta)$ can be chosen as the exact known mode in the y-direction. This allows the computation of infinitely many modes $\phi(\xi)$ in the x-direction by following only **Step 1**, without requiring further iterations. Similarly, if $\phi_{n_x}(\xi)$ is selected as the exact known mode in the x-direction, infinitely many modes $\psi(\eta)$ in the y-direction can be computed by following only **Step 2**, without iterations.

For example, if the (n_x, n_y)-th mode is nonzero and obtained through the iteration procedure, then based on $\psi_{n_y}(\eta)$, the modes $(1, n_y)$, $(2, n_y)$, ..., (∞, n_y) of the plate can be computed without further iteration. Similarly, based on $\phi_{n_x}(\xi)$, the modes $(n_x, 1)$, $(n_x, 2)$, ..., (n_x, ∞) of the plate can be determined. That is, only one iteration procedure is required to calculate all frequencies of the plate, which helps reduce the computational cost.

4. Numerical Results

This section presents the numerical validation of the proposed method for classic boundary conditions and elastically restrained boundary conditions. For all numerical calculations, the initial integral parameters are assumed as $S_1^{(0)} = 1$, $S_2^{(0)} = 1$, $S_3^{(0)} = 1$, and $S_4^{(0)} = 10$ in the y-direction, serving as the starting point of **Step 1** for any mode in all BCs. In this section, the interval between the upper and lower bounds of the non-dimensional frequency parameter, $2a\Delta\Omega$, is set to 0.005, defining the error range. According to our numerical calculations, two iteration cycles are sufficient to meet the convergence requirement for most cases, with at most three cycles needed when applying the iterative procedure in Section 3.2.1.

4.1. Classical boundary conditions

In this subsection, the proposed method is validated by comparison with the extended SOV method [27]. The properties of the orthotropic plate, consistent with those in [27], are as follows: $E_1 = 185\text{GPa}$, $E_2 = 10.5\text{GPa}$, $G_{12} = 7.3\text{GPa}$, $\rho = 1600\ \text{kg}\,\text{m}^{-1}$, and $\nu_{12} = 0.28$.

The initial guess for $S_1^{(0)}, S_2^{(0)}, S_3^{(0)}$, and $S_4^{(0)}$ is assumed to be $1, 1, 1, 10$ for all boundary conditions and mode orders. This differs from the iterative SOV method 26, which requires a different initial guess for each mode order. The translational springs (k_ξ^v) and rotational springs (k_ξ^r) along all edges can be set to zero or infinity (represented as $1 \times 10^{15}\ \text{N}\,\text{m}^{-1}$ in the numerical calculations of this study) to obtain different classic boundary conditions.

The results for SSSS, SCSF, GCGC, CCCC, SSCC, SCCC, GGCC, CCFF, CFCF, CFFF, and FFFF boundary conditions are presented in Tables 1 to 3. These results demonstrate high accuracy compared to the extended SOV method, with errors remaining smaller than the interval between the upper and lower bounds (0.005). The frequency parameters in both directions are equal ($2a\Omega_x - 2a\Omega_y = 0$) in almost all cases, with a few exceptions where $2a\Omega_x - 2a\Omega_y = 0.005$. Figure 2 shows the first six nonzero mode shapes of a square orthotropic plate with FFFF boundary conditions.

4.2. Rotationally restrained boundary conditions

In this subsection, rectangular orthotropic plates with rotationally restrained edges ($k_\xi^v = k_\eta^v = \infty$) are validated. The rotational stiffness coefficients are defined as:

$$r_\xi = \frac{2ak_\xi^r}{D_{11}}, \tag{64a}$$

$$r_\eta = \frac{2bk_\eta^r}{D_{22}}. \tag{64b}$$

The first example considers a square isotropic plate with all four edges rotationally restrained. The vertical translational springs along the four edges are numerically set as $k_{\xi=-1}^v = k_{\xi=1}^v = k_{\eta=-1}^v = k_{\eta=1}^v = 1 \times 10^{12}\ \mathrm{N\,m^{-1}}$. The material properties are given as $D_{11} = D_{22} = D_3$ and $v_{12} = v_{21} = 0.3$.

Table 4 presents the frequency parameter $2a\Omega$ for different rotational stiffness coefficients $r_\xi = r_\eta$ with values $0.1, 1, 10, 100$, and 1000. Notably, when $r_\xi = r_\eta = 0$ and $r_\xi = r_\eta = \infty$, the boundary conditions correspond to SSSS and CCCC, respectively.

Interestingly, the results indicate that the frequencies Ω_x and Ω_y are not strictly equal for some mode shapes under rotationally restrained boundary conditions. The actual frequency Ω lies between Ω_x and Ω_y, which may be attributed to the fact that Ω_x and Ω_y satisfy Rayleigh's principle in Equation (3), representing the weak-form governing equations, but do not necessarily satisfy the strong-form governing equations in Equation (1). For a physical problem with exact solutions, both Equations (1) and (3) must be satisfied. If this condition is not met, applying Equation (3) still provides a viable approach for approximating the exact solution of the plate. Thus, the exact frequency can be estimated as $\Omega = (\Omega_x + \Omega_y)/2$. As shown in Table 4, the maximum difference between Ω and the solutions reported in 31 is less than 1.3%. Figure 3 illustrates the variation in mode shapes corresponding to the fundamental natural frequency as the rotational stiffness $r_\xi = r_\eta$ increases from zero to ∞, transitioning the boundary conditions from SSSS to CCCC.

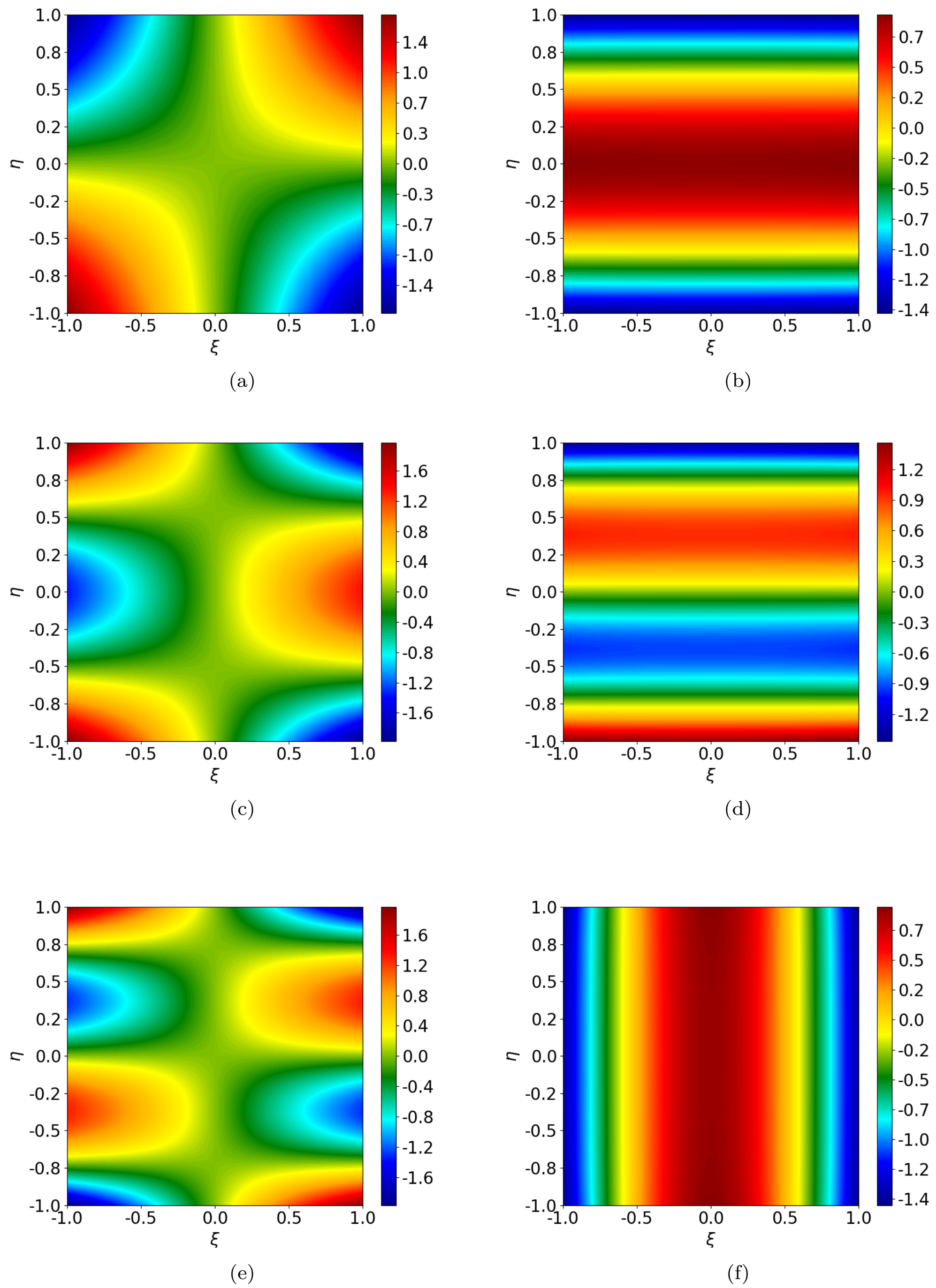

Figure 2: The first six nonzero mode shapes of a square orthotropic plate with FFFF boundary conditions: (a) the first mode; (b) the second mode; (c) the third mode; (d) the fourth mode; (e) the fifth mode; (f) the sixth mode.

Table 1: The first seven frequency parameter $2a\Omega$ of of orthotropic rectangular plates with SSSS, SCSF and GCGC boundary conditions.

			$2a\Omega_x = 2a\Omega_y = 2a\sqrt[4]{\rho h\omega^2/D_{11}}$						
BCs	α	Mode	1	2	3	4	5	6	7
SSSS	0.5	Mode number	(1,1)	(1,2)	(1,3)	(1,4)	(1,5)	(1,6)	(1,7)
		extended SOV 27	3.1807	3.3190	3.5938	4.0135	4.5495	5.1635	5.8265
		Present	3.1825	3.3225	3.5975	4.0175	4.5525	5.1625	5.8275
	1	Mode number	(1,1)	(1,2)	(1,3)	(2,1)	(1,4)	(2,2)	(2,3)
		extended SOV 27	3.3190	4.0135	5.1635	6.3615	6.5200	6.6379	7.1876
		Present	3.3175	4.0175	5.1625	6.3625	6.5175	6.6375	7.1875
	1.5	Mode number	(1,1)	(1,2)	(2,1)	(2,2)	(1,3)	(2,3)	(1,4)
		extended SOV 27	3.5938	5.1635	6.4698	7.1876	7.2331	8.5389	9.4352
		Present	3.5975	5.1675	6.4725	7.1875	7.2325	8.5375	9.4375
SCSF	0.5	Mode number	(1,1)	(1,2)	(1,3)	(1,4)	(1,5)	(1,6)	(1,7)
		extended SOV 27	3.1516	3.2451	3.4588	3.8131	4.2950	4.8711	5.5087
		Present	3.1525	3.2475	3.4575	3.8175	4.2925	4.8725	5.5075
	1	Mode number	(1,1)	(1,2)	(1,3)	(1,4)	(2,1)	(2,2)	(2,3)
		extended SOV 27	3.1908	3.6428	4.5972	5.8599	6.3033	6.4901	6.9177
		Present	3.1925	3.6425	4.5975	5.8575	6.3025	6.4925	6.9175
	1.5	Mode number	(1,1)	(1,2)	(1,3)	(2,1)	(2,2)	(2,3)	(1,4)
		extended SOV 27	3.2710	4.3430	6.2157	6.3337	6.8043	7.8718	8.3518
		Present	3.2725	4.3425	6.2175	6.3325	6.8025	7.8725	8.3525
GCGC	0.5	Mode number	(1,1)	(1,2)	(1,3)	(2,1)	(2,2)	(1,4)	(2,3)
		extended SOV 27	1.1544	1.9166	2.6835	3.1983	3.3890	3.4501	3.7372
		Present	1.1525	1.9175	2.6825	3.1975	3.3875	3.4525	3.7375
	1	Mode number	(1,1)	(2,1)	(1,2)	(2,2)	(1,3)	(2,3)	(3,1)
		extended SOV 27	2.3087	3.4900	3.8331	4.4682	5.3669	5.7736	6.3967
		Present	2.3075	3.4875	3.8325	4.4675	5.3675	5.7725	6.3975
	1.5	Mode number	(1,1)	(2,1)	(1,2)	(2,2)	(3,1)	(3,2)	(1,3)
		extended SOV 27	3.4631	4.1353	5.7497	6.0981	6.6049	7.6449	8.0504
		Present	3.4625	4.1325	5.7475	6.0975	6.6075	7.6425	8.0525

Table 2: The first seven frequency parameter $2a\Omega$ of of orthotropic rectangular plates with CCCC, SSCC, SCCC and GGCC boundary conditions.

			$2a\Omega_x = 2a\Omega_y = 2a\sqrt[4]{\rho h \omega^2 / D_{11}}$						
BCs	α	Mode	1	2	3	4	5	6	7
CCCC	0.5	Mode number	(1,1)	(1,2)	(1,3)	(1,4)	(1,5)	(1,6)	(1,7)
		extended SOV 27	4.7500	4.8208	4.9682	5.2177	5.5791	6.0430	6.5892
		Present	4.7475	4.8225	4.9725	5.2175	5.5825	6.0425	6.5875
	1	Mode number	(1,1)	(1,2)	(1,3)	(1,4)	(2,1)	(2,2)	(2,3)
		extended SOV 27	4.8579	5.3546	6.2819	7.4972	7.9193	8.1490	8.6054
		Present	4.8575	5.3575	6.2875	7.4975	7.9175	8.1475	8.6075
	1.5	Mode number	(1,1)	(1,2)	(2,1)	(1,3)	(2,2)	(2,3)	(1,4)
		extended SOV 27	5.1581	6.5412	8.0409	8.4945	8.7204	9.9793	10.6460
		Present	5.1575	6.5375	8.0425	8.4975	8.7175	9.9775	10.6425
SSCC	0.5	Mode number	(1,1)	(1,2)	(1,3)	(1,4)	(1,5)	(1,6)	(1,7)
		extended SOV 27	3.9542	4.0520	4.2525	4.5785	5.0254	5.5682	6.1789
		Present	3.9575	4.0525	4.2475	4.5775	5.0225	5.5725	6.1825
	1	Mode number	(1,1)	(1,2)	(1,3)	(1,4)	(2,1)	(2,2)	(2,3)
		extended SOV 27	4.0745	4.6606	5.7009	6.9940	7.1396	7.3894	7.8881
		Present	4.0775	4.6625	5.7025	6.9925	7.1375	7.3875	7.8875
	1.5	Mode number	(1,1)	(1,2)	(2,1)	(1,3)	(2,2)	(2,3)	(1,4)
		extended SOV 27	4.3602	5.8384	7.2531	7.8560	7.9481	9.2515	10.0366
		Present	4.3625	-5.8325	7.2525	7.8575	7.9525	9.2525	10.0325
SCCC	0.5	Mode number	(1,1)	(1,2)	(1,3)	(1,4)	(1,5)	(1,6)	(1,7)
		extended SOV 27	3.9596	4.0745	4.3027	4.6606	5.1361	5.7009	6.3271
		Present	3.9575	4.0725	4.3025	4.6625	5.1325	5.7025	6.3325
	1	Mode number	(1,1)	(1,2)	(1,3)	(2,1)	(1,4)	(2,2)	(2,3)
		extended SOV 27	4.1349	4.8478	5.9805	7.1541	7.3192	7.4478	8.0121
		Present	4.1325	4.8475	5.9825	7.1525	7.3175	7.4475	8.0125
	1.5	Mode number	(1,1)	(1,2)	(2,1)	(2,2)	(1,3)	(2,3)	(3,1)
		extended SOV 27	4.5824	6.2766	7.3116	8.1528	8.3705	9.5986	10.3507
		Present	4.5825	6.2775	7.3125	8.1525	8.3725	9.5975	10.3525
GGCC	0.5	Mode number	(1,1)	(1,2)	(1,3)	(1,4)	(1,5)	(1,6)	(1,7)
		extended SOV 27	2.3750	2.4841	2.7895	3.2946	3.9226	4.6123	5.3326
		Present	2.3725	2.4875	2.7925	3.2975	3.9225	4.6075	5.3325
	1	Mode number	(1,1)	(1,2)	(1,3)	(2,1)	(2,2)	(1,4)	(2,3)
		extended SOV 27	2.4290	3.1410	4.4293	5.5202	5.7315	5.8801	6.2606
		Present	2.4325	3.1425	4.4325	5.5225	5.7325	5.8775	6.2625
	1.5	Mode number	(1,1)	(1,2)	(2,1)	(2,2)	(1,3)	(2,3)	(3,1)
		extended SOV 27	2.5790	4.2472	5.5565	6.1533	6.4347	7.5231	8.6732
		Present	2.5825	4.2475	5.5575	6.1525	6.4325	7.5225	8.6725

Table 3: The first seven nonzero frequency parameter $2a\Omega$ of of orthotropic rectangular plates with CCFF, CFCF, CFFF and FFFF boundary conditions.

			$2a\Omega_x = 2a\Omega_y = 2a\sqrt[4]{\rho h\omega^2/D_{11}}$						
BCs	α	Mode	1	2	3	4	5	6	7
CCFF	0.5	Mode number	(1,1)	(1,2)	(1,3)	(1,4)	(1,5)	(1,6)	(2,1)
		extended SOV 27	1.8978	2.0905	2.4925	3.0563	3.7110	4.4117	4.7029
		Present	1.8975	2.0925	2.4925	3.0575	3.7125	4.4125	4.7025
	1	Mode number	(1,1)	(1,2)	(1,3)	(2,1)	(2,2)	(1,4)	(2,3)
		extended SOV 27	1.9930	2.7895	4.0733	4.7338	5.0652	5.5128	5.7419
		Present	1.9925	2.7875	4.0725	4.7325	5.0675	5.5125	5.7425
	1.5	Mode number	(1,1)	(1,2)	(2,1)	(2,2)	(1,3)	(2,3)	(3,1)
		extended SOV 27	2.1780	3.7411	4.7931	5.5758	5.8895	7.0263	7.9006
		Present	2.1775	3.7425	4.7925	5.5725	5.8875	7.0275	7.9025
CFCF	0.5	Mode number	(1,1)	(1,2)	(1,3)	(1,4)	(1,5)	(1,6)	(1,7)
		extended SOV 27	4.7297	4.7427	4.7881	4.8819	5.0478	5.3072	5.6694
		Present	4.7275	4.7425	4.7875	4.8825	5.0475	5.3075	5.6675
	1	Mode number	(1,1)	(1,2)	(1,3)	(1,4)	(1,5)	(1,6)	(2,1)
		extended SOV 27	4.7295	4.7817	5.0012	5.5348	6.4407	7.6182	7.8523
		Present	4.7275	4.7825	5.0025	5.5325	6.4425	7.6175	7.8525
	1.5	Mode number	(1,1)	(1,2)	(1,3)	(1,4)	(2,1)	(2,2)	(2,3)
		extended SOV 27	4.7292	4.8458	5.4221	6.7635	7.8518	7.9470	8.3021
		Present	4.7275	4.8475	5.4225	6.7625	7.8525	7.9475	8.3025
CFFF	0.5	Mode number	(1,1)	(1,2)	(1,3)	(1,4)	(1,5)	(1,6)	(1,7)
		extended SOV 27	1.8751	1.9439	2.1679	2.5657	3.1106	3.7486	4.4382
		Present	1.8775	1.9425	2.1675	2.5675	3.1125	3.7475	4.4375
	1	Mode number	(1,1)	(1,2)	(1,3)	(1,4)	(2,1)	(2,2)	(2,3)
		extended SOV 27	1.8750	2.1242	2.9077	4.1319	4.6937	4.8226	5.2263
		Present	1.8775	2.1225	2.9075	4.1325	4.6925	4.8225	5.2275
	1.5	Mode number	(1,1)	(1,2)	(1,3)	(2,1)	(2,2)	(2,3)	(1,4)
		extended SOV 27	1.8750	2.3402	3.8522	4.6935	4.9753	5.8314	5.9292
		Present	1.8775	2.3425	3.8525	4.6925	4.9775	5.8325	5.9275
FFFF	0.5	Mode number	(1,3)	(2,2)	(1,4)	(2,3)	(1,5)	(2,4)	(2,5)
		extended SOV 27	1.1540	1.4858	1.9157	2.1704	2.6821	2.7881	3.4093
		Present	1.1525	1.4875	1.9175	2.1725	2.6825	2.7875	3.4075
	1	Mode number	(2,2)	(1,3)	(2,3)	(1,4)	(2,4)	(3,1)	(3,2)
		extended SOV 27	2.1311	2.3082	3.2734	3.8320	4.4962	4.7298	4.9138
		Present	2.1325	2.3075	3.2725	3.8325	4.4975	4.7275	4.9125
	1.5	Mode number	(2,2)	(1,3)	(2,3)	(3,1)	(3,2)	(1,4)	(3,3)
		extended SOV 27	2.6277	3.4625	4.2915	4.7296	5.1259	5.7485	6.1588
		Present	2.6275	3.4625	4.2925	4.7275	5.1275	5.7475	6.1575

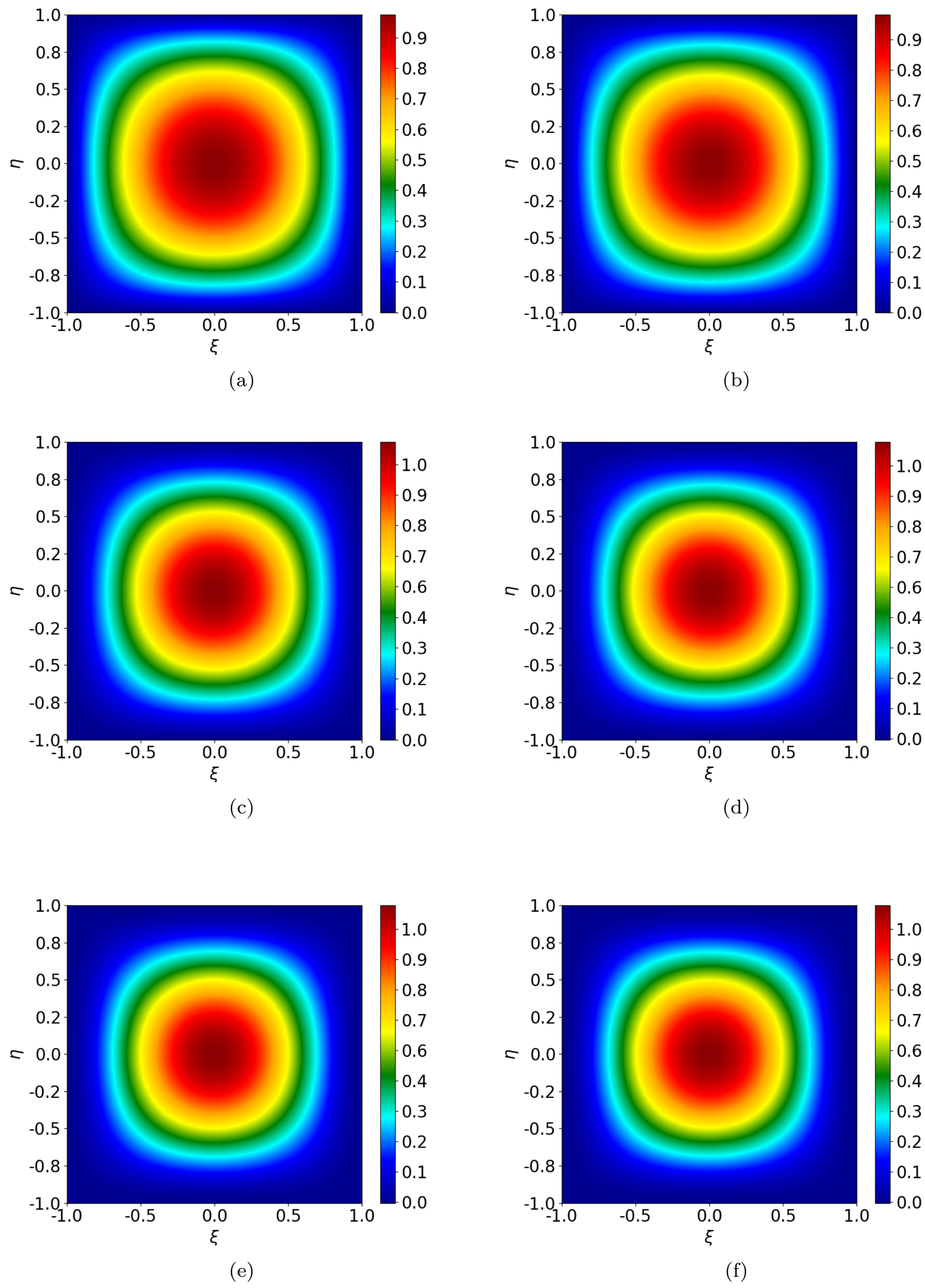

Figure 3: The first mode shape of a square isotropic plate with all four edges rotationally restrained: (a) $r_\xi = r_\eta = 0$; (b) $r_\xi = r_\eta = 1$; (c) $r_\xi = r_\eta = 10$; (d) $r_\xi = r_\eta = 20$; (e) $r_\xi = r_\eta = 100$; (f) $r_\xi = r_\eta = \infty$.

Table 4: The first six frequency parameters, $2a\Omega = 2a\sqrt[4]{\rho h \omega^2 / D_{11}}$, of a square isotropic plate with all four edges rotationally restrained, where $k^r_{\xi=-1} = k^r_{\xi=1} = k^r_{\eta=-1} = k^r_{\eta=1}$.

		$2a\Omega$					
$r_\xi = r_\eta$	Mode	1	2	3	4	5	6
0.1	Mode number	(1,1)	(1,2)	(2,1)	(2,2)	(1,3)	(3,1)
	Ref.20	4.454	6.992	7.045	8.890	9.782	9.960
	Ref.31	4.465	7.039	7.039	8.897	9.945	9.945
	Present (Ω)	4.463	7.035	7.035	8.893	9.945	9.945
	Present (Ω_x)	4.463	7.028	7.043	8.893	9.938	9.953
	Present (Ω_y)	4.463	7.043	7.028	8.893	9.953	9.938
	Difference (%)	0.044	0.056	0.056	0.044	0.000	0.000
1	Mode number	(1,1)	(1,2)	(2,1)	(2,2)	(3,1)	(1,3)
	Ref.20	4.529	7.008	7.136	8.936	9.787	10.036
	Ref.31	4.637	7.155	7.155	8.991	10.029	10.030
	Present (Ω)	4.648	7.160	7.160	8.993	10.030	10.033
	Present (Ω_x)	4.648	7.098	7.223	8.993	10.093	9.968
	Present (Ω_y)	4.648	7.223	7.098	8.993	9.968	10.098
	Difference (%)	0.237	0.069	0.069	0.022	0.009	0.029
10	Mode number	(1,1)	(1,2)	(2,1)	(2,2)	(1,3)	(3,1)
	Ref.31	5.346	7.768	7.768	9.537	10.552	10.563
	Present (Ω)	5.413	7.835	7.835	9.598	10.615	10.618
	Present (Ω_x)	5.413	7.718	7.953	9.598	10.448	10.782
	Present (Ω_y)	5.413	7.953	7.718	9.598	10.782	10.453
	Difference (%)	1.253	0.862	0.862	0.639	0.597	0.520
100	Mode number	(1,1)	(1,2)	(2,1)	(2,2)	(1,3)	(3,1)
	Ref.20	5.895	8.326	8.422	10.167	10.957	11.297
	Ref.31	5.901	8.442	8.442	10.253	11.307	11.333
	Present (Ω)	5.913	8.450	8.450	10.258	11.333	11.333
	Present (Ω_x)	5.913	8.428	8.473	10.258	11.293	11.373
	Present (Ω_y)	5.913	8.473	8.478	10.258	11.373	11.293
	Difference (%)	0.203	0.094	0.094	0.048	0.229	0.000
1000	Mode number	(1,1)	(1,2)	(2,1)	(2,2)	(1,3)	(3,1)
	Ref.31	6.011	8.585	8.585	10.424	11.495	11.522
	Present (Ω)	5.988	8.553	8.553	10.388	11.470	11.470
	Present (Ω_x)	5.988	8.553	8.553	10.388	11.463	11.478
	Present (Ω_y)	5.988	8.553	8.553	10.388	11.478	11.463
	Difference (%)	0.382	0.372	0.372	0.345	0.217	0.451

The next example considers a rectangular orthotropic plate with three simply supported edges ($k^r_{\xi=-1} = k^r_{\xi=1} = k^r_{\eta=1} = 0$), while the edge at $\eta = -1$ is rotationally restrained. The material properties are consistent with those in 31, where $2D_{11} = 2D_{22} = D_3$ and $\nu_{12} = \nu_{21} = 0.3$. Table 5 shows the fundamental frequency results for different length ratios (b/a), comparing them with those reported in 31. The maximum observed difference is 0.8% when $r_{\eta=-1} = 10$. Furthermore, Figure 4 shows how the fundamental mode shape of the square orthotropic plate evolves as the rotational spring stiffness $k^r_{\eta=-1}$ increases.

In certain numerical calculations involving rotationally restrained boundary conditions, the variables α_1 and α_2 may take complex values rather than being purely real. Consequently, the mode shape coefficients A_1, A_2, B_1, and B_2 become complex-valued, leading to $\mathbf{R}$ and $\mathbf{Q}^{-1}$ being complex matrices. However, the mode shapes $\phi(\xi)$ and $\psi(\eta)$ remain real-valued, and the dynamic stiffness matrix $\mathbf{K} = \mathbf{R}\mathbf{Q}^{-1}$ is a real symmetric matrix. Thus, the frequency Ω can be obtained by solving $\mathbf{K}$ using the refined W-W algorithm provided in this study, which avoids solving the eigenvalue equations in both the real and complex domains.

Table 5: Fundamental frequency parameter $2a\Omega = 2a\sqrt[4]{\rho h\omega^2/D_{11}}$ of rectangular orthotropic plates with three edges simply supported ($k^r_{\xi=-1} = k^r_{\xi=1} = k^r_{\eta=1} = 0$) and the edge at $\eta = -1$ rotationally restrained.

		$2a\Omega$				
b/a	$r_{\eta=-1}$	Ref.31	Present (Ω)	Present (Ω_x)	Present (Ω_y)	Difference (%)
0.5	0	7.530	7.523	7.523	7.523	0.092
	1	7.690	7.700	7.588	7.813	0.130
	10	8.250	8.308	8.198	8.418	0.703
	∞	8.705	8.695	8.695	8.695	0.114
1.0	0	4.917	4.918	4.918	4.918	0.020
	1	4.954	4.960	4.933	4.988	0.121
	10	5.114	5.128	5.088	5.168	0.273
	∞	5.289	5.278	5.278	5.278	0.207
1.5	0	4.126	4.128	4.128	4.128	0.048
	1	4.139	4.138	4.128	4.148	0.024
	10	4.202	4.208	4.188	4.228	0.142
	∞	4.292	4.288	4.288	4.288	0.093

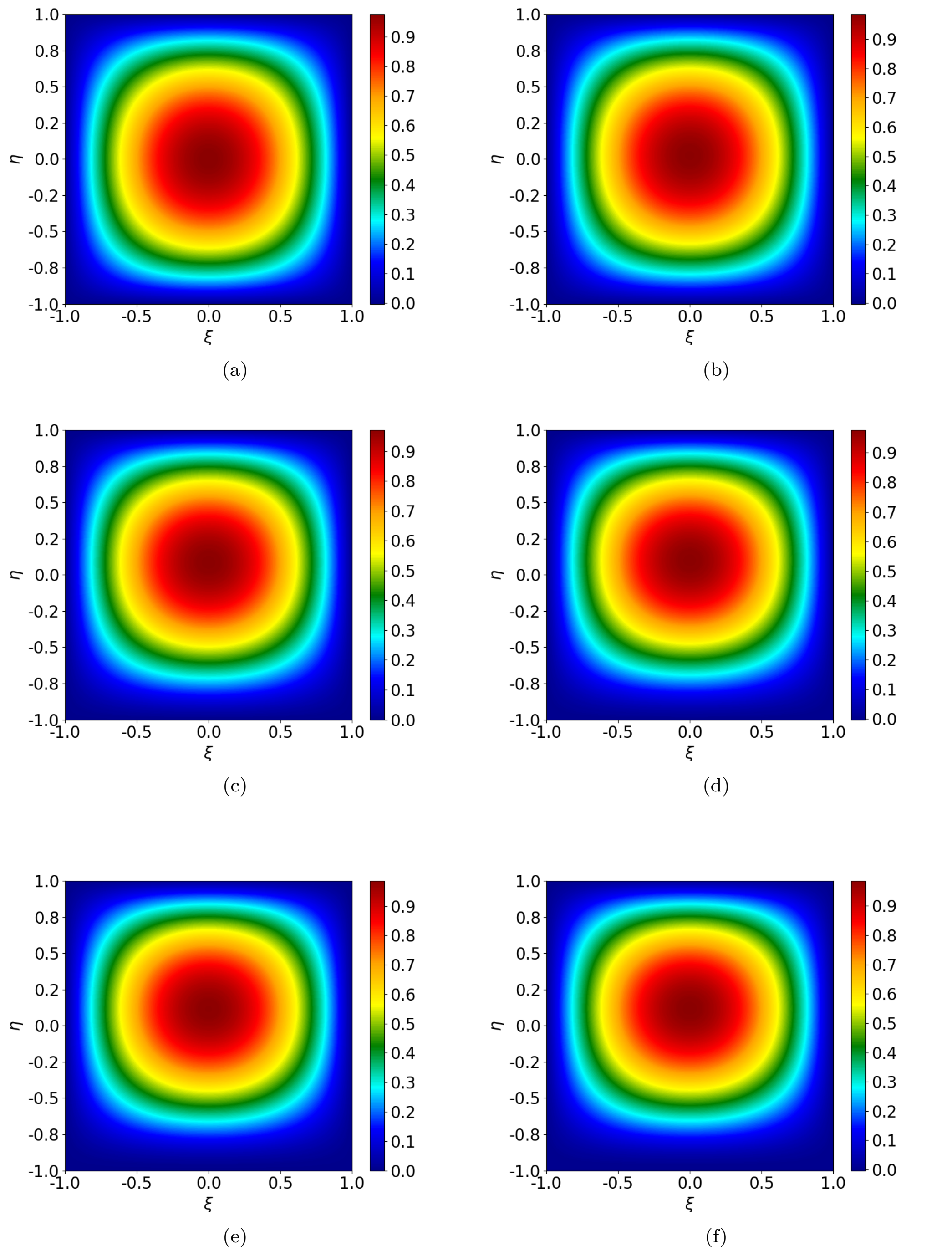

Figure 4: The first mode shape of a square orthotropic plate with the edge at $\eta = -1$ rotationally restrained: (a) $r_{\eta=-1} = 0$; (b) $r_{\eta=-1} = 1$; (c) $r_{\eta=-1} = 10$; (d) $r_{\eta=-1} = 20$; (e) $r_{\eta=-1} = 100$; (f) $r_{\eta=-1} = \infty$.

5. Conclusion

In this study, the dynamic stiffness matrix (DSM) based on the extended separation-of-variable (SOV) mode functions has been developed for the vibration analysis of an orthotropic rectangular plate with general homogeneous boundary conditions.

Based on the Rayleigh quotient, the governing equation of the plate, along with the shear force and bending moment equilibrium related to the boundary conditions, are derived. The extend-SOV type solutions obtained from the governing equation are then used to develop the dynamic stiffness matrices by applying the boundary conditions. Instead of solving eigenvalue equations involving highly nonlinear and transcendental functions derived from the determinant of the dynamic stiffness matrix, a refined W-W algorithm based on the 'hypothetical structure method' is developed to address this eigenvalue problem. The challenge of determining the fully clamped frequencies using the W-W algorithm is resolved by finding the simply supported frequencies, whose closed-form expression can be easily derived based on the SOV method. Due to the improved W-W algorithm and the concise SOV-form solutions, the process of solving the dynamic stiffness matrix becomes more systematic and efficient.

Classical boundary conditions, such as guided, simply supported, clamped, and free edges, can be realized by setting the translational springs (k_ξ^v) and rotational springs (k_ξ^r) along the plate edges to either zero or infinity. Numerical results confirm that accurate solutions are obtained for these boundary conditions. Despite some approximations in certain elastically restrained boundary conditions, the maximum percentage error across all numerical experiments remains within 1.25%. This may occur because the SOV-form solutions used are derived from the weak-form governing equation, which is based on Rayleigh's principle.

Since the SOV-form solution $\phi(\xi)\psi(\eta)$ consists of only a single term, unlike the infinite series expansions used in the traditional DSM, each eigenvalue solution can be explicitly expressed. This suggests the potential for obtaining concise and closed-form solutions for assembled plate structures compared to traditional DSM methods.

Appendix A Integral parameters

The integral parameters S_1, S_2, S_3, and S_4 are defined as follows:

$$\begin{aligned}
S_1 &= \int_0^1 \psi^2 \, d\eta \\
&= (B_1^2 + B_2^2 - B_3^2 + B_4^2) + \frac{-B_1^2 + B_2^2}{2\alpha_2}\sin(2\alpha_2) + \frac{B_3^2 + B_4^2}{2\beta_2}\sinh(2\beta_2) \\
&\quad + \frac{4(\alpha_2 B_2 B_4 + \beta_2 B_1 B_3)}{\alpha_2^2 + \beta_2^2}\sin(\alpha_2)\cosh(\beta_2) \\
&\quad + \frac{4(-\alpha_2 B_1 B_3 + \beta_2 B_2 B_4)}{\alpha_2^2 + \beta_2^2}\cos(\alpha_2)\sinh(\beta_2).
\end{aligned} \tag{A.1}$$

$$\begin{aligned}
S_2 &= \int_0^1 \left(\psi \frac{d^2\psi}{d\eta^2}\right) d\eta \\
&= \left(-\alpha_2^2 B_1^2 - \alpha_2^2 B_2^2 - \beta_2^2 B_3^2 + \beta_2^2 B_4^2\right) \\
&\quad + \frac{\alpha_2(B_1^2 - B_2^2)}{2}\sin(2\alpha_2) + \frac{\beta_2(B_3^2 + B_4^2)}{2}\sinh(2\beta_2) \\
&\quad + \frac{2(-\alpha_2^2 + \beta_2^2)(\alpha_2 B_2 B_4 + \beta_2 B_1 B_3)}{\alpha_2^2 + \beta_2^2}\sin(\alpha_2)\cosh(\beta_2) \\
&\quad + \frac{2(-\alpha_2^2 + \beta_2^2)(-\alpha_2 B_1 B_3 + \beta_2 B_2 B_4)}{\alpha_2^2 + \beta_2^2}\cos(\alpha_2)\sinh(\beta_2).
\end{aligned} \tag{A.2}$$

$$\begin{aligned}
S_3 &= \int_0^1 \left(\frac{d\psi}{d\eta}\right)^2 d\eta \\
&= \alpha_2^2 B_1^2 + \alpha_2^2 B_2^2 + \beta_2^2 B_3^2 - \beta_2^2 B_4^2 \\
&\quad + \frac{\alpha_2(B_1^2 - B_2^2)}{2}\sin(2\alpha_2) + \frac{\beta_2(B_3^2 + B_4^2)}{2}\sinh(2\beta_2) \\
&\quad + \frac{4\alpha_2\beta_2(\alpha_2 B_1 B_3 - \beta_2 B_2 B_4)}{\alpha_2^2 + \beta_2^2}\sin(\alpha_2)\cosh(\beta_2) \\
&\quad + \frac{4\alpha_2\beta_2(\alpha_2 B_2 B_4 + \beta_2 B_1 B_3)}{\alpha_2^2 + \beta_2^2}\cos(\alpha_2)\sinh(\beta_2).
\end{aligned} \tag{A.3}$$

$$
\begin{aligned}
S_4 &= \int_0^1 \left(\frac{d^2\psi}{d\eta^2}\right)^2 d\eta \\
&= \left(\alpha_2^4 B_1^2 + \alpha_2^4 B_2^2 - \beta_2^4 B_3^2 + \beta_2^4 B_4^2\right) \\
&\quad + \frac{\alpha_2^3(-B_1^2 + B_2^2)}{2}\sin(2\alpha_2) + \frac{\beta_2^3(B_3^2 + B_4^2)}{2}\sinh(2\beta_2) \\
&\quad + \frac{4\alpha_2^2\beta_2^2(-\alpha_2 B_2 B_4 - \beta_2 B_1 B_3)}{\alpha_2^2 + \beta_2^2}\sin(\alpha_2)\cosh(\beta_2) \\
&\quad + \frac{4\alpha_2^2\beta_2^2(\alpha_2 B_1 B_3 - \beta_2 B_2 B_4)}{\alpha_2^2 + \beta_2^2}\cos(\alpha_2)\sinh(\beta_2)
\end{aligned}
\tag{A.4}
$$

The integral parameters T_1, T_2, T_3, and T_4 can be obtained by replacing B_1 to B_4 by A_1 to A_4, respectively, and α_2 and β_2 by α_1 and β_1, respectively.

References

[1] Banerjee, J., Papkov, S., Liu, X., Kennedy, D., 2015. Dynamic stiffness matrix of a rectangular plate for the general case. Journal of Sound and Vibration 342, 177–199. doi:10.1016/j.jsv.2014.12.031.

[2] Banerjee, J.R., 1997. Dynamic stiffness formulation for structural elements: a general approach. Computers & Structures 63, 101–103. doi:10.1016/S0045-7949(96)00326-4.

[3] Biancolini, M.E., Brutti, C., Reccia, L., 2005. Approximate solution for free vibrations of thin orthotropic rectangular plates. Journal of Sound and Vibration 288, 321–344. doi:10.1016/j.jsv.2005.01.005.

[4] Boscolo, M., Banerjee, J., 2011. Dynamic stiffness elements and their applications for plates using first order shear deformation theory. Computers & Structures 89, 395–410. doi:10.1016/j.compstruc.2010.11.005.

[5] Fazzolari, F., Boscolo, M., Banerjee, J., 2013. An exact dynamic stiffness element using a higher order shear deformation theory for free vibration analysis of composite plate assemblies. Composite Structures 96, 262–278. doi:10.1016/j.compstruct.2012.08.033.

[6] Ghorbel, O., Casimir, J.B., Hammami, L., Tawfiq, I., Haddar, M., 2015. Dynamic stiffness formulation for free orthotropic plates. Journal of Sound and Vibration 346, 361–375. doi:10.1016/j.jsv.2015.02.020.

[7] Gorman, D.J., 2005. Free in-plane vibration analysis of rectangular plates with elastic support normal to the boundaries. Journal of Sound and Vibration 285, 941–966. doi:10.1016/j.jsv.2004.09.017.

[8] Han, F., Dan, D., Cheng, W., Zang, J., 2018. An improved wittrick-williams algorithm for beam-type structures. Composite Structures 204, 560–566. doi:10.1016/j.compstruct.2018.07.108.

[9] Kantorovich, L.V., Krylov, V.I., 1958. Approximate Methods of Higher Analysis. Interscience Publishers, New York.

[10] Kerr, A.D., 1968. An extension of the kantorovich method. Quarterly of Applied Mathematics 26, 219–229. doi:10.1090/qam/99857.

[11] Khov, H., Li, W.L., Gibson, R.F., 2009. An accurate solution method for the static and dynamic deflections of orthotropic plates with general boundary conditions. Composite Structures 90, 474–481. doi:10.1016/j.compstruct.2009.04.020.

[12] Laura, P.A., Saffell Jr, B.F., 1967. Study of small-amplitude vibrations of clamped rectangular plates using polynomial approximations. The Journal of the Acoustical Society of America 41, 836–839. doi:10.1121/1.1910414.

[13] Leissa, A.W., 1973. The free vibration of rectangular plates. Journal of Sound and Vibration 31, 257–293. doi:10.1016/S0022-460X(73)80371-2.

[14] Levy, M., 1899. Sur l'équilibre élastique d'une plaque rectangulaire. Comptes Rendus Acad. Sci. Paris 129, 535–539.

[15] Li, R., Zhong, Y., Tian, B., Liu, Y., 2009a. On the finite integral transform method for exact bending solutions of fully clamped orthotropic rectangular thin plates. Applied Mathematics Letters 22, 1821–1827. doi:10.1016/j.aml.2009.07.003.

[16] Li, W.L., 2004. Vibration analysis of rectangular plates with general elastic boundary supports. Journal of Sound and Vibration 273, 619–635. doi:10.1016/S0022-460X(03)00562-5.

[17] Li, W.L., Zhang, X., Du, J., Liu, Z., 2009b. An exact series solution for the transverse vibration of rectangular plates with general elastic boundary supports. Journal of Sound and Vibration 321, 254–269. doi:10.1016/j.jsv.2008.09.035.

[18] Liu, X., Banerjee, J., 2015. An exact spectral-dynamic stiffness method for free flexural vibration analysis of orthotropic composite plate assemblies–part i: Theory. Composite Structures 132, 1274–1287. doi:10.1016/j.compstruct.2015.07.020.

[19] Liu, X., Banerjee, J., 2016. Free vibration analysis for plates with arbitrary boundary conditions using a novel spectral-dynamic stiffness method. Computers & Structures 164, 108–126. doi:10.1016/j.compstruc.2015.11.005.

[20] Mukhopadhyay, M., 1979. Free vibration of rectangular plates with edges having different degrees of rotational restraint. Journal of Sound and Vibration 67, 459–468.

[21] Navier, L., 1823. Extrait des recherches sur la flexion des plans elastiques. Bull. Sci. Soc. Philomat. , 95–102.

[22] Timoshenko, S., 1940. Theory of Plates and Shells. McGraw-Hill Book Company.

[23] Wittrick, W.H., Williams, F.W., 1971. A general algorithm for computing natural frequencies of elastic structures. The Quarterly Journal of Mechanics and Applied Mathematics 24, 263–284. doi:10.1093/qjmam/24.3.263.

[24] Xing, Y., Li, G., Yuan, Y., 2022. A review of the analytical solution methods for the eigenvalue problems of rectangular plates. International Journal of Mechanical Sciences 221, 107171. doi:10.1016/j.ijmecsci.2022.107171.

[25] Xing, Y., Liu, B., 2009a. New exact solutions for free vibrations of rectangular thin plates by symplectic dual method. Acta Mechanica Sinica 25, 265–270. doi:10.1007/s10409-008-0208-4.

[26] Xing, Y., Sun, Q., Liu, B., Wang, Z., 2018. The overall assessment of closed-form solution methods for free vibrations of rectangular thin

plates. International Journal of Mechanical Sciences 140, 455–470. doi:10.1016/j.ijmecsci.2018.03.013.

[27] Xing, Y., Wang, Z., 2020a. An extended separation-of-variable method for the free vibration of orthotropic rectangular thin plates. International Journal of Mechanical Sciences 182, 105739. doi:10.1016/j.ijmecsci.2020.105739.

[28] Xing, Y., Wang, Z., 2020b. An improved separation-of-variable method for the free vibration of orthotropic rectangular thin plates. Composite Structures 252, 112664. doi:10.1016/j.compstruct.2020.112664.

[29] Xing, Y.F., Liu, B., 2009b. New exact solutions for free vibrations of thin orthotropic rectangular plates. Composite Structures 89, 567–574. doi:10.1016/j.compstruct.2008.11.010.

[30] Yuan, S., Ye, K., Williams, F., 2004. Second order mode-finding method in dynamic stiffness matrix methods. Journal of Sound and Vibration 269, 689–708. doi:10.1016/S0022-460X(03)00126-3.

[31] Zhang, S., Xu, L., Li, R., 2019. New exact series solutions for transverse vibration of rotationally-restrained orthotropic plates. Applied Mathematical Modelling 65, 348–360. doi:10.1016/j.apm.2018.08.033.

[32] Zhong, W.X., 1995. A new systematic methodology for theory of elasticity. Dalian University of Technology Press, Dalian , 182–187.

[33] Zhong, Y., Zhao, X.F., Li, R., 2013. Free vibration analysis of rectangular cantilever plates by finite integral transform method. International Journal for Computational Methods in Engineering Science and Mechanics 14, 221–226. doi:10.1080/15502287.2012.711424.